

# Structural and energetic properties of nickel clusters: $2 \leq N \leq 150$

Valeri G. Grigoryan\* and Michael Springborg†

*Physical Chemistry, University of Saarland, 66123 Saarbrücken, Germany*

(Dated: December 23, 2021)

## Abstract

The four most stable structures of  $\text{Ni}_N$  clusters with  $N$  from 2 to 150 have been determined using a combination of the embedded-atom method in the version of Daw, Baskes and Foiles, the *variable metric/quasi-Newton* method, and our own *Aufbau/Abbau* method. A systematic study of energetics, structure, growth, and stability of also larger clusters has been carried through without more or less severe assumptions on the initial geometries in the structure optimization, on the symmetry, or on bond lengths. It is shown that cluster growth is predominantly icosahedral with *islands* of *fcc*, *tetrahedral* and *decahedral* growth. For the first time in unbiased computations it is found that  $\text{Ni}_{147}$  is the multilayer (third Mackay) icosahedron. Further, we point to an enhanced ability of *fcc* clusters to compete with the icosahedral and decahedral structures in the vicinity of  $N = 79$ . In addition, it is shown that conversion from the *hcp/anti-Mackay* kind of icosahedral growth to the *fcc/Mackay* one occurs within a transition layer including several cluster sizes. Moreover, we present and apply different analytical tools in studying structural and energetic properties of such a large class of clusters. These include means for identifying the overall shape, the occurrence of atomic shells, the similarity of the clusters with, e.g., fragments of the *fcc* crystal or of a large icosahedral cluster, and a way of analysing whether the  $N$ -atom cluster can be considered constructed from the  $(N - 1)$ -atom one by adding an extra atom. In addition, we compare in detail with results from chemical-probe experiment. Maybe the most central result is that first for clusters with  $N$  above 80 general trends can be identified.

PACS numbers: (2003) 61.46.+w, 36.40.-c, 68.65.-k, 31.15.Ct

---

\* Corresponding author. e-mail: vg.grigoryan@mx.uni-saarland.de

† e-mail: m.springborg@mx.uni-saarland.de

## I. INTRODUCTION

Clusters are important materials both from the point of view of basic research and from an application point of view. Their, partly controllable, unique physical and chemical properties can be related to the large surface-to-volume ratio or to finite-size or quantum-confinement effects. These properties make them interesting for use in, e.g., nanoelectronics and in catalysis.

The central issue is to understand and predict how the properties of interest depend on the size of the cluster. However, addressing this question is complicated by a number of serious problems. First, clusters contain typically from some 10s to several 100s of atoms, so that they are neither small, well-characterized molecules, nor macroscopic, approximately infinite crystals. Moreover, in experimental studies, one often considers an ensemble of more or less mono-disperse clusters whose size distribution is largely unknown. Second, experimental and theoretical studies focus often on different systems: in experiment the clusters may be dispersed in some solvent and may possess surfactants and only sometimes are produced in the gas phase, whereas isolated clusters in this gas phase almost exclusively are the subject of theoretical studies. Third, in theoretical works the fairly large size of the individual clusters makes it necessary to invoke one or more approximations: either highly accurate methods on selected clusters with pre-chosen structures are applied, or less accurate, parameterized methods are used on more different clusters, but also then the structures are often chosen ‘reasonably’.

In this work we shall present results of our theoretical studies on  $\text{Ni}_N$  clusters with  $N$  up to 150. Our approach is based on the approximate embedded-atom method (EAM) in calculating the total energy of a given structure and we shall show that this method provides a good compromise between accuracy and computational speed. Moreover, we have used our own *Aufbau/Abbau* method in determining the structures of the lowest total energies. Ni clusters provide one of the most studied sets of clusters and, therefore, is an excellent system for exploring new theoretical or experimental approaches. This is our main reason for focusing on that system. Moreover, through our unbiased structure-optimization approach we are able to identify the structures of more low-energy structures for each size, and, simultaneously, obtain structure and total energy for all values of  $N$  up to  $N = 150$ , whereby size-specific properties can be extracted.

Once the structure of a given cluster has been chosen, the variational principle allows for a systematic improvement of the calculated electronic properties. A similar approach does not exist for the structural properties where one, instead, has to use more or less biased methods for determining the structure of the lowest total energy. Here, three issues make such theoretical studies very demanding: first, the computational efforts for a single structure scales with  $N$  to some power from 2 and upwards; second, the number of structural parameters that have to be determined scale linearly with  $N$ ; and, third, the number of meta-stable structures scales faster than any power of  $N$ .<sup>1</sup> Therefore, any theoretical study employs one or more approximation that may or may not be crucial.

Accordingly, parameter-free calculations on  $\text{Ni}_N$  clusters<sup>2,3,4,5,6,7</sup> have been applied mainly for smaller clusters as well as on single, high-symmetric, larger ones. Alternatively, unbiased structure optimizations for larger clusters are all based on more approximate total-energy methods like the EAM or related methods,<sup>8,9,10,11,12,13,14,15,16,17</sup> whereby only for  $N \leq 55$  the structure has been optimized completely unbiased, or the very simple  $n$ -body Gupta,<sup>18,19,20,21,22</sup> Sutton-Chen,<sup>23</sup> Finnis-Sinclair,<sup>25</sup> Murrell-Mottram,<sup>26</sup> or Morse potential<sup>27</sup> has been used, whereby unbiased structure optimizations up to  $N = 80$  have been carried through.<sup>23</sup> Only for very simple and material-unspecific potentials, like the Lennard-Jones potential, largely unbiased structure optimizations up to  $N \sim 150$  have been carried through.<sup>24</sup> Finally,  $\text{Ni}_N$  clusters have also been studied with a tight-binding method,<sup>28</sup> whereby the structure only for clusters with  $N \leq 10$  was optimized unbiased.

Of the experimental studies on  $\text{Ni}_N$  clusters,<sup>29,30,31,32,33,34,35,36,37</sup> the chemical-probe experiments<sup>29,30,31,32,33,34,35,36</sup> have given very valuable information on the structure of the smaller clusters. On the other hand, results for medium and large Ni clusters,<sup>37</sup> obtained by performing near-threshold photoionization and time-of-flight mass spectroscopy can be used in identifying particularly stable clusters and, subsequently, in providing information on growth modes.

From the earlier studies on nickel clusters it has been found that highly stable clusters occur for  $N = 13$  and  $N = 55$  for which the structures are multilayer icosahedra, i.e., the first and second Mackay icosahedra. Moreover, in several theoretical studies<sup>17,22,23</sup> a *fcc* truncated octahedron was found for  $\text{Ni}_{38}$  which is in accord with experimental results. Thus, it can be assumed that for these three cluster sizes a ‘structural consensus’ has been achieved, which in turn provides a useful check for any further study. On the other hand,

for  $N = 75$  some theoretical studies<sup>22,23</sup> have predicted Marks decahedron to be the most stable structure, in disagreement with experiment. Moreover, the cluster growth pattern for intermediate sizes, i.e., for  $13 < N < 55$  and for  $N > 55$ , remains unclear and the obtained results seem to depend strongly on the used approach.

In the present study the structure and the energetics of the four most stable isomers for small and medium-sized  $\text{Ni}_N$  clusters with  $N$  from 2 to 150 have been determined for each cluster size using a combination of the EAM (for calculation of the total energy for a given structure), the *variable metric/quasi-Newton* method (for the determination of local total-energy minima), and our own *Aufbau/Abbau* method (for the determination of the global total-energy minimum). Except for two cases ( $N = 75$  and  $N = 104$ ; here we included the decahedron as a starting configuration) our structure-determination is completely unbiased. In particular, as we shall see, it is important to go beyond  $N = 80$  (the upper limit in the earlier unbiased structure-optimizations) in order to identify growth patterns. In addition, we shall present results for clusters that are obtained as relaxed spherical parts of the *fcc* crystal with  $N$  up to some 1000s.

The paper is organized as follows. In Sec. II we briefly outline the embedded-atom method, and in Sec. III we present our structural-determination methods. The main results are given in Sec. IV, and a brief summary is offered in Sec. V. Finally, for the sake of completeness we mention that some preliminary results on clusters with up to  $N = 100$  and results for the energetically lowest isomer were presented earlier<sup>38,39</sup> and in the discussion of the results we shall use eV and Å as units of energy and length, respectively.

## II. EMBEDDED-ATOM METHOD

We use the EAM of Daw, Baskes, and Foiles<sup>40,41,42,43</sup> for the calculation of the total energy of a given cluster with a given structure. The main idea of Daw and Baskes<sup>40,41</sup> is to split the total energy of a (metallic) system of interest into two components. The embedding energy is obtained by considering each atom as an impurity embedded into a host provided by the rest of the atoms. The remaining part is written as a sum of pair potentials. Accordingly,

$$E_{\text{tot}} = \sum_i F_i(\rho_i^h) + \frac{1}{2} \sum_{i,j (i \neq j)} \phi_{ij}(R_{ij}), \quad (1)$$

where  $\rho_i^h$  is the local electron density at site  $i$ ,  $F_i$  is the embedding energy, i.e., the energy required to embed an atom into this density, and  $\phi_{ij}$  is a short-range potential between atoms  $i$  and  $j$  separated by the distance  $R_{ij}$ ,

$$\phi_{ij} = \frac{Z_i(R_{ij}) Z_j(R_{ij})}{R_{ij}}. \quad (2)$$

Here the effective charges  $Z_i(R_{ij})$  and  $Z_j(R_{ij})$  depend on  $R_{ij}$ . The local electron density at site  $i$  is assumed being a superposition of atomic electron densities

$$\rho_i^h = \sum_{j(\neq i)} \rho_i^a(R_{ij}), \quad (3)$$

where  $\rho_i^a(R_{ij})$  is the spherically averaged atomic electron density provided by atom  $j$  at the distance  $R_{ij}$ .

In the present approach, the atomic densities have been taken from Hartree-Fock calculations of Refs. [44,45]. Moreover, adjustable parameters that define  $F_i$  and  $\phi_{ij}$  have been obtained by fitting to known bulk properties such as sublimation energy, lattice constant, the heat of solution of binary alloys and, additionally, to the universal equation of Rose,<sup>46</sup> which describes the sublimation energy of the most metals as a function of lattice constant. The values for  $\rho_i^a$ ,  $F_i$  and  $Z_i$  that we have used are available in numerical form for Ni, Cu, Ag, Au, Pd and Pt.<sup>47</sup>

Our main reason for choosing the EAM is that the EAM provides a computationally efficient, parameterized many-particle method that allows for many calculations of also larger systems. Thus, with this method we can perform unbiased structure optimizations for clusters with well above 100 atoms, which is not possible using more accurate, parameter-free methods. Moreover, by comparing (see Sec. IV A) with results of more accurate studies for the smallest clusters we can estimate the accuracy of the method. Since the method has been developed first of all for macroscopic metallic systems, in particular the smallest clusters may be those for which the largest inaccuracies show up.

### III. OPTIMIZATION OF THE STRUCTURE

Using expression (1) we can calculate the total energy of any cluster with any structure as a function of atomic coordinates  $\{\vec{R}_i\}$ ,  $E_{\text{tot}}(\vec{R}_1, \vec{R}_2, \dots, \vec{R}_N)$ . In order to obtain the closest local total-energy minimum we use the *variable metric/quasi-Newton* method.<sup>48</sup> We found that this was significantly more efficient than the *conjugate gradient* method.

For searching the global minima we have developed our own *Aufbau/Abbau* method. It consists of the following steps:

1) We consider two cluster sizes with  $N$  and  $N + K$  atoms with  $K \simeq 5 - 10$ . For each of those we study a set of randomly generated structures,  $N_{\text{ran}} \simeq 1000$ . Using the *quasi-Newton* method the  $N_{\text{ran}}$  relaxed structures are identified and the structures of the lowest total energy selected. Each of the  $N_{\text{ran}}$  starting structures for a cluster with  $M$  atoms was generated using a random-number generator for positions within a sphere or a cube of volume  $V_{cl} = (p \cdot b_{nn})^3 M$ , where  $b_{nn} = 2.49 \text{ \AA}$  is the nearest-neighbor distance of bulk Ni and  $p = 0.8, 1.0, 1.2$ , i.e. we considered slightly compressed, normal, and slightly expanded structures. We included the constraints that the smallest allowed inter-atomic distance was  $0.5b_{nn}$  and each atom has to interact with at least two others.

2) One by one, each of the  $M$  atoms is displaced randomly, and the closest local minima is determined. If the new structure has a lower total energy than the original one, this new one is kept, and the old one discarded. This is repeated approximately 500 – 1000 times (depending on cluster size).

3) This leaves us with two ‘source’ clusters,  $\text{Ni}_N$  and  $\text{Ni}_{N+K}$  with their lowest total energies. One by one an atom is added at a random position to the structure with  $N$  atoms (many hundred times for each size), and the structures are relaxed. In parallel, one by one an atom is removed from the structure with  $N + K$  atoms — for each intermediate cluster with  $N'$  atoms we consider *all*  $N' + 1$  possible configurations, that one can obtain by removing one atom from the  $\text{Ni}_{N'+1}$  cluster. From the two series of structures for  $N \leq M \leq N + K$  those structures of the lowest energies are chosen and these are used as seeds for a new set of calculations. First, when no lower total energies are found, it is assumed that the structures of the global-total-energy minima have been identified, and we proceed to larger clusters.

Moreover, by keeping information on not only the single energetically lowest isomer, but more low-lying ones, we have been able to identify the energetically four lowest-lying isomers.

Our method combines randomness with regularity and is significantly more efficient compared to the case when only random starting geometries are used. In addition, it is completely unbiased. However, as for any structure-determination method, there is no guarantee that we have identified the true global total-energy minima, although we believe that we in most cases have very good candidates. But, unfortunately, in two cases,  $N = 75$  and  $N = 104$  (both cases correspond to decahedral structures, which often have been difficult to

find in unbiased structure optimizations), our approach failed and we had to include that in our study explicitly, and in another,  $N = 38$ , we only got the previously obtained structure after considerably more attempts than otherwise used. We add that similar problems have been observed and analysed in studies on Lennard-Jones clusters.<sup>49</sup>

## IV. RESULTS AND DISCUSSIONS

### A. Small clusters — accessing the accuracy

The smallest clusters, i.e.,  $\text{Ni}_N$  for  $2 \leq N \leq 13$ , provide an excellent test for our approach of two reasons: The clusters are so small that the number of (meta-)stable structures is small, which in turn means that the global total-minimum within a given approach can be identified. And since the EAM has its foundations in considerations for infinite, extended metallic systems with largely delocalized electrons, the small clusters should be those that with most difficulties can be treated by our approach. Therefore, we have in Table I tabulated our obtained structural parameters for  $2 \leq N \leq 8$  and  $N = 13$  in comparison with results of other theoretical or experimental studies.

The table shows that the structure, here given through the average bond length  $\langle r \rangle$ , is most often given within a couple of % of the results of experiment or of parameter-free electronic-structure calculations. Moreover, none of the other parameterized methods, i.e., the tight-binding approach or model potentials of the Sutton-Chen, Gupta, or effective-medium type, gives results that are systematically more accurate than our approach does. This is important since for the larger clusters that we shall discuss here it is not possible to apply accurate parameter-free methods when simultaneously attempting to optimize the structure.

The table also shows that the relative ordering of the different isomers may differ for different methods. Hence, for  $N = 7$  most parameterized methods predict the  $D_{5h}$  isomer to have a lower total energy than the  $C_{3v}$  structure, whereas experiment and parameter-free theoretical studies predict a reversed ordering. Therefore, it can be important to calculate more different, energetically low-lying isomers when studying theoretically the properties of not very small clusters — identifying a different isomer as the one of the lowest total energy may suggest a significant disagreement between different studies.

In order to emphasize this point further we show in Fig. 1 the structures of the two energetically lowest isomers for  $6 \leq N \leq 13$ . It is very clearly seen that in some cases the two isomers are indeed very different and identifying the ‘wrong’ one as the most stable one may give unexpected results.

It may also surprise that for the two isomers for  $N = 7$  that look very different we find a total-energy difference of only 0.03 eV/atom. To our knowledge there exist two DFT calculations of  $\text{Ni}_7$  cluster.<sup>5,6</sup> Both studies predict for the two energetically lowest isomers a capped octahedron and a pentagonal bipyramid, respectively. The corresponding average binding energy per atom are found to differ by only 0.05–0.07 eV/atom, i.e., very similar to our findings.

Table I and Fig. 1 give one further result for  $N = 7$ :  $\text{Ni}_7$  is the smallest cluster that incorporates the fivefold symmetry axis, an important element of icosahedral and decahedral symmetries.

For  $N = 8$  our two energetically lowest isomers differ in energy by 0.016 eV/atom, in good agreement with the value of 0.02 eV/atom found by Desmarais *et al.* in a DFT study.<sup>6</sup> There are some fundamental differences between different *ab initio* studies on  $\text{Ni}_8$  cluster.<sup>3,4,6,7</sup> According to one study<sup>4</sup> a cube is the most stable structure for  $\text{Ni}_8$ , whereas in other studies<sup>6,7</sup> a cube was only the 5th isomer. Further, in another work<sup>7</sup> the second isomer was found to be a bicapped trigonal prism ( $C_{2v}$ ) and a capped pentagonal bipyramid was only isomer number four. Micheline *et al.*<sup>3</sup> has found for the eight-atom nickel cluster only one isomer with the tetrahedral symmetry  $T_d$ . This GGA result is inconsistent with all other studies. It seems that the LSDA calculations of Desmarais *et al.*<sup>6</sup> have the best agreement with both experimental and semiempirical studies.

To our best knowledge there are only DFT studies<sup>2,4</sup> on  $\text{Ni}_N$ ,  $9 \leq N \leq 13$ , for  $N = 13$ . At  $N = 13$  the first Mackay icosahedron ( $I_h$ ) is constructed. The second isomer is 1.16 eV less stable. This is a rather large value and the icosahedron as the most stable structure for  $\text{Ni}_{13}$  was found almost in all theoretical studies (the only exception being an extended-Hückel study<sup>52</sup>). Once again we obtain good structural agreement with *ab initio* studies.<sup>2,4</sup> The obtained bond lengths of 2.36 (center to vertex) and 2.48 Å (vertex to vertex) agree well with those derived by Calleja *et al.*,<sup>2</sup> i.e.,  $2.41 \pm 0.03$  and  $2.53 \pm 0.03$  Å, and with those of Reuse and Khanna,<sup>4</sup> i.e., 2.23 and 2.34 Å, respectively. Furthermore, when comparing the differences in the binding energies per atom between the  $\text{Ni}_{13}$  and  $\text{Ni}_2$  clusters, our value



of 1.525 eV/atom agrees very well with the corresponding value of 1.558 eV/atom obtained using the self-consistent DFT program SIESTA.<sup>2</sup>

Closing this subsection we emphasize that for our purpose, the calculation of energetic and structural properties of  $\text{Ni}_N$  clusters, the present EAM approach appears to be sufficiently accurate.

## B. Energetic properties

In Fig. 2 we show the binding energy per atom for the optimized clusters for the four energetically lowest isomers together with the binding energy per atom for clusters that were constructed as relaxed, spherical parts of the *fcc* crystal structure (with an atom at the center of the sphere) for  $N$  up to almost 2600. With few expectations the four total-energy curves are so close that their difference can not be resolved in the figure. On the other hand, except for  $N = 79$ , the *fcc*-derived clusters lie all below the other structures, indicating that for  $N$  up to around 150 the *fcc* structure is not playing a significant role as a structural motif (an exception occurs for  $N = 38$  for a fragment of the *fcc* crystal with the center not at an atom — this case is not shown in the figure). Fig. 2(b) shows that the apparent saturation is not real: first when considering considerably larger clusters, the convergence towards an average binding energy around 4.45 eV/atom can be recognized.

In order to identify the particularly stable clusters we shall consider two criteria. First, a cluster may be considered very stable if its binding energy per atom is much larger than that of the two neighboring clusters. This can be quantified through the stability function,  $E_{\text{tot}}(N + 1.1) + E_{\text{tot}}(N - 1.1) - 2E_{\text{tot}}(N.1)$ , where  $E_{\text{tot}}(N.k)$  is the total energy of the energetically  $k$ -lowest isomer of the  $\text{Ni}_N$  cluster. This function, that has maxima for particularly stable clusters, is shown in Fig. 3. Here we can identify a large number of particularly stable clusters, i.e., so-called magic clusters. These are found for  $N = 4, 6, 10, 13, 15, 19, 23, 26, 28, 32, 36, 39, 43, 46, 49, 55, 58, 61, 64, 67, 71, 75, 77, 79, 83, 86, 89, 92, 95, 99, 101, 104, 108, 110, 114, 116, 119, 122, 125, 127, 129, 131, 137, \text{ and } 147$ . The most pronounced peaks occur at  $N = 13, 19, 23, 46, 49, 55, 71, 75, 116, 131, 137, \text{ and } 147$  and most of them contain an odd number of atoms and, as seen in Table II, these clusters possess high symmetry, including the highest icosahedral symmetry for  $\text{Ni}_{13}$ ,  $\text{Ni}_{55}$ , and  $\text{Ni}_{147}$ .

According to our other criterion for a particularly stable cluster, such a cluster occurs if

the energy difference between the two energetically lowest isomers  $E_{\text{tot}}(N.2) - E_{\text{tot}}(N.1)$  is large. This energy difference together with the energy differences to the energetically higher ones are shown in Fig. 4. It is striking that the energetically higher-lying isomers become energetically less and less separated and, as seen when comparing with Fig. 3, many of the clusters that are particularly stable according to the first criterion is it also according to the second one.

### C. Structural properties

A central issue of our work is to identify general properties of the  $\text{Ni}_N$  clusters from the large amount of information that we have obtained from the calculations. Instead of discussing the individual clusters, in particular their structure (a brief summary of the structures is given in the Appendix), we shall introduce different quantities that are devised to reduce the available information to some few key numbers.

First we shall consider the overall shape of the clusters. As we discussed in our earlier report,<sup>39</sup> it is useful to examine the  $3 \times 3$  matrix containing the elements

$$I_{st} = \frac{1}{u_l^2} \sum_{n=1}^N (R_{n,s} - R_{0,s})(R_{n,t} - R_{0,t}) \quad (4)$$

with  $u_l = 1\text{\AA}$  being our length unit, and  $s$  and  $t$  being  $x$ ,  $y$ , and  $z$ , and with

$$\vec{R}_0 = \frac{1}{N} \sum_{n=1}^N \vec{R}_n \quad (5)$$

being the center of the cluster. The three eigenvalues of this matrix,  $I_{\alpha\alpha}$ , can be used in separating the clusters into being overall spherical (all eigenvalues are identical), more cigar-like shaped (one eigenvalue is large, the other two are small), or more lens-shaped (two large and one small eigenvalue). Moreover, the average of the three eigenvalues,  $\langle I_{\alpha\alpha} \rangle$ , is a measure of the overall extension of the cluster. Finally, for a homogeneous sphere with  $N$  atoms, the eigenvalues scale like  $N^{5/3}$ . Therefore, we show in Fig. 5 quantities related to these eigenvalues but scaled by  $N^{-5/3}$ .

In the figure we see that only some few clusters have an overall spherical shape (these are found for the energetically lowest isomer for  $N = 4, 6, 13, 26, 28, 38, 55$ , and  $147$  and for the next one for  $N = 54, 79$ , and  $92$ ), which all correspond to high-symmetry isomers (cf. Table II) and, for the lowest-energy isomer, also to the class of magic clusters. Moreover, it

is interesting to notice that the average value follows more or less the same curve for all four isomers, i.e., the more compact ones (with relative low average value) are found for  $N$  just above 50 and above 140). Also the largest differences follow more or less the same curve, except for some few cases mainly for  $N$  below 40. Therefore, except when the eigenvalues all are very similar (i.e., the largest difference is very small, which occurs for  $N$  around 50, 100, and 140), the overall shape (i.e., lens- or cigar-like) is the same for all four isomers.

In our earlier work<sup>39</sup> we showed that the structural development of the isomer of the lowest total energy with advantage could be monitored through so-called similarity functions. Thus, for a given cluster  $\text{Ni}_N$  we define a radial distance for each of the atoms

$$r_n = |\vec{R}_n - \vec{R}_0| \quad (6)$$

and sort these in increasing order.

Simultaneously we consider a large fragment of a *fcc* crystal or, alternatively, a large cluster of icosahedral symmetry. Also for these we define a radial distance for each atom,  $r'_n$ , that also are sorted. In order to compare the given cluster with any of those systems we calculate subsequently

$$q = \left[ \frac{1}{N} \sum_{n=1}^N (r_n - r'_n)^2 \right]^{1/2}, \quad (7)$$

giving the similarity function

$$S = \frac{1}{1 + q/u_l} \quad (8)$$

( $u_l = 1\text{\AA}$ ), which approaches 1 if the  $\text{Ni}_N$  cluster is very similar to the reference system. In Fig. 6 we show the resulting functions in four cases, i.e., when comparing with the relaxed  $\text{Ni}_{309}$  cluster of icosahedral symmetry, and when comparing with three fragments of the *fcc* crystal differing in the position of the center (the position of an atom, the middle of a nearest-neighbor bond, and the center of the cube, respectively).

We see that both clusters that clearly resemble *fcc* fragments and such that resemble icosahedral clusters can be identified. Of obvious reasons, the latter is the case for  $N$  around 13, 55, and 147, but it is interesting to notice that these clusters are not singular: clusters with a large similarity to icosahedral clusters are found over a larger range of clusters ( $\sim 10$ ) around the truly icosahedral cluster. Similarly, clusters that are close to being fragments of the *fcc* crystal can be identified around  $N = 13, 28, 38$ , and 79. Moreover, it is surprising to observe that all four isomers for a given size show very similar similarity functions.

Also the radial distances themselves can give some interesting information. These are shown in Fig. 7 for the four different isomers as functions of cluster size. Up to  $N$  around 40, only few trends can be identified (with the exception of  $N = 13$ ), but for  $N$  just above 50 a clear tendency towards shell-construction can be seen. Whereas this transition towards shell-construction is fairly smooth as a function of cluster size, independent of whether we start from the larger or the smaller clusters, in the range  $75 \leq N \leq 80$  abrupt changes occur also towards some shell-construction. That this size range is special shall be discussed in more detail below. Also for  $N$  close to 115 this tendency is seen, but most dramatic are the results for clusters around 140 and above where, for all four isomers, a very clear shell-construction is identified. Comparing with Fig. 6 we see that this is correlated to the construction of icosahedral-like structures. Thus, since the infinite crystal possesses the *fcc* structure, the clear shell-construction in this size range will have to disappear again for larger clusters.

In total, it can not surprise that when analysing the structures of the individual clusters in detail we can identify many structural motifs that are characteristic for clusters of particularly high stability also for clusters with somewhat different sizes. Moreover, such an analysis<sup>54</sup> shows also that many of our structures for the smaller  $N$  (these are the only ones that have been the subject of earlier unbiased structure-optimizations) are close to those that have been found in earlier studies. Here, however, we shall largely omit the discussion of the individual structures but instead explore the more general trends.

In Fig. 8 we show some few quantities related to the structure of the clusters, i.e., coordination numbers and average bond lengths. Here, we define two atoms as being bonded if their interatomic distance is less than 3.00 Å, which is the average of the nearest-neighbor distance (2.49 Å) and the next-nearest-neighbor distance (3.52 Å) in bulk Ni. Moreover, we distinguish between inner atoms with a coordination number of 12 or larger and surface atoms with a coordination number less than 12.

Fig. 8(a) shows the average coordination number as function of  $N$ , where an obvious increase as function of size is observed, but with additional oscillations in particular for the smallest clusters. This function shows clearly a saturation towards the bulk limit of 12, although one has to remember that even for the largest cluster of our study 94 out of 150 atoms are characterized as surface atoms.

Fig. 8(b) shows the minimum atomic coordination for each cluster size from the range

$N = 2-150$ , which is useful information for chemical-probe experiments due to the enhanced chemical activity of clusters containing low-coordination atoms. In addition, the existence of low-coordination atoms (i.e., coordinations of 3 or 4) could point to the occurrence of a cluster growth, where extra atoms are added to the surface of the cluster, whereas the higher minimum-atomic-coordination numbers (*e.g.* 5 or 6) could indicate a growth where atoms are inserted inside the cluster, or, alternatively, upon a strong rearrangement of the surface atoms. These considerations follow the so-called "maximizing the minimum coordination".<sup>16,17</sup>

Fig. 8(c) shows the average bond length as function of cluster size. The dashed line corresponds to the bulk value of 2.49 Å. The average bond length for all the structures with the exception of Ni<sub>31</sub>, Ni<sub>35</sub>, Ni<sub>71</sub>, and Ni<sub>86</sub> is smaller than the bulk value. Such a reduction is in accordance with the results of most other theoretical studies, but it is interesting to observe that this property approaches the bulk value faster than the other quantities of the figure.

Important experimental work in the determination of the structure of individual Ni<sub>N</sub> clusters has been presented by Riley *et al.*<sup>30,31,32,33,34,35</sup> using chemical-probe experiments. Thereby, the number of N<sub>2</sub> molecules that is bonded to a given cluster is determined, and in order to relate this number to the structure of the cluster, the following empirical rules have been formulated:<sup>30,31,32</sup> (i) nickel atoms with a coordination of four and less will bind two nitrogen molecules at saturation, (ii) nickel atoms with coordination of five to eight will bind only one nitrogen molecule at saturation, (iii) nickel atoms with a coordination of nine will bind one nitrogen molecule weakly or not at all (this kind of binding has not been observed<sup>32</sup> for  $N > 49$ ), and (iv) nickel atoms with a coordination more than nine do not bind any nitrogen molecules. These rules allow us in turn to estimate the number of N<sub>2</sub> molecules that will bond to a given cluster. We stress that the chemical-probe experiments provide information on the complete system, i.e., cluster plus adsorbants, whereas we consider the naked clusters. Although this difference may result in some deviations between theory and experiment, a comparison should give useful information on the clusters. This is supported by the studies of Parks *et al.*<sup>30,31</sup> that show that in many cases the structures of naked and N<sub>2</sub>-covered clusters are very similar.

Doing so, we obtain the results of Fig. 9, where we also compare with the results of other theoretical works. The experimental work covers the range  $3 \leq N \leq 72$ , whereas the former

theoretical works cover  $4 \leq N \leq 80$  (Ref. [23]),  $3 \leq N \leq 23$  (Ref. [25]), and  $24 \leq N \leq 55$  (Ref. [17]), obtained using the Sutton-Chen potential,<sup>23</sup> the Finnis-Sinclair potential,<sup>25</sup> and the effective-medium theory.<sup>17</sup> Fig. 9(a), where we show the results for the whole range of our study, i.e.,  $2 \leq N \leq 150$ , shows an interesting aspect that obviously is beyond most of the previous experimental and theoretical studies, i.e., that up to around  $N \simeq 55$  the number of binding sites increases more rapidly with  $N$  than for  $N$  above  $\sim 55$ , i.e., the curve is roughly two piecewise linear curves. The experimental studies [cf. Figs. 9(d) and (e)] do in fact show a small tendency in this direction, which, on the other hand, is not found in the earlier theoretical work [cf. Fig. 9(c)]. Figs. 9(b)-(e) show a comparison of the experimental results with those of the four different theoretical studies to this issue. It is clear that our approach is at least as accurate as any of the other theoretical ones. Moreover, the Sutton-Chen potential seems to predict a larger scatter of the number of binding sites as a function of size compared to any other approach.

Whereas icosahedral motifs are found to play an important role for very many values of  $N$ , we found that for  $N$  around 75 also other structural motifs are important. The chemical-probe results for  $N_2$  uptake, both the experimental ones (notice, however, that the experimental studies are limited to  $N \leq 72$ ) and the simulated, theoretical ones, suggest also that in this range of  $N$  values more structural motifs compete: for these values of  $N$  the results of Fig. 9 are particularly scattered. Moreover, as we shall see in the next subsection, also growth processes suggest that these  $N$  values are special. Therefore, we shall study the structural properties of those clusters in some more detail.

For cluster sizes ranging between 70 and 80 atoms two more closed-shell structures other than icosahedral ones can be identified, i.e., the (2,2,2) Marks decahedron (giving a 75-atom cluster) and a 79-atom *fcc* cluster, which is the truncated centered octahedron. Due to their quasi-spherical shape they have a particularly low surface energy. Moreover, the cluster sizes between 70 and 80 are very different from the values of closed-shell icosahedral clusters that have 55 or 147 atoms. Accordingly, one may expect a strong competition between these three main morphologies in this size range. Our calculations support this suggestion. Fig. 10 shows the lowest total energies for the decahedral and *fcc* clusters relative to the icosahedral ones for  $72 \leq N \leq 82$ . The Marks decahedron and its derivatives dominate over the icosahedral structures for  $73 \leq N \leq 79$ . At  $N = 79$  both decahedral and *fcc* motifs are more stable than the icosahedral one. The decahedron at  $N = 79$  is only 0.04 eV more

stable than the truncated octahedron. Finally, three of four lowest-energy isomers at  $N = 75$  are decahedra and for  $N = 76 - 78$  there are only decahedral clusters among the four first isomers.

This result suggests that a fundamental structural change takes place for  $N$  around 75. This, however, is only partly the case: for larger  $N$  values the icosahedral packing is again stabilized (an exception occurs for  $N$  around 104, where decahedral structures are found). In order to verify this we computed the total energies for several optimized closed *fcc* and decahedral structures, i.e., truncated noncentered octahedra for  $N = 116$  and 140, a noncentered octahedron and a (3,2,2) Marks decahedron for  $N = 146$ , and a cuboctahedron and an Ino decahedron for  $N = 147$ . In all cases the icosahedral structures were found to have lower total energies. The *fcc* clusters for  $N = 116$ , 140 and 146 and *m*-Dh<sub>146</sub> were 0.85, 2.01, 5.64 and 2.29 eV, respectively, less stable than the icosahedral-like structures. The three-shell Mackay icosahedron was 5.69 and 4.71 eV more stable than the cuboctahedron and the Ino decahedron, accordingly. Thus, our calculations point strongly to icosahedral growth up to cluster sizes of at least 150. This statement is supported by mass-spectroscopy studies of nickel clusters<sup>37</sup> which suggest icosahedral growth over a wide cluster-size region from 50 to 800.

#### D. Growth patterns

One of the central issues is to identify how clusters grow, i.e., whether some fundamental principles determine how (and whether) the cluster with  $N$  atoms is derived from the one with  $N - 1$  atoms. We shall here study this issue from a completely static point of view, i.e., dynamic and kinetic effects, that most likely are important in experiment, will be neglected here. Basic information about this issue is given by the structures of the magic clusters. The majority of the structures of these are icosahedral. Thus our study supports predominantly icosahedral growth of nickel clusters. There are two different ways of icosahedral growth. Thus, the first Mackay icosahedron, Ih<sub>13</sub>, contains 20 triangular faces joined by 30 edges and 12 vertices. In the first case, MIC/Mackay or *fcc* covering,<sup>11,55,56,57,58</sup> additional surface atoms are placed on top of the edges and the vertices. This kind of growth results ultimately in the second Mackay icosahedron, Ih<sub>55</sub>. Another possibility, the TIC/polyicosahedral<sup>11,55</sup> or *hcp* or face-capping growth (see Ref. [56] and references therein), corresponds to adding

atoms on top of the atoms at the center of each face ( $T$  sites) which leads, after complete covering, to the 45-atom rhombic tricontahedron. The TIC structures are the structures with the shorter average bond length, but at the same time they possess the larger strain energy. They are favored at the beginning of a covering until some critical size (depending on details of the atom-atom interaction<sup>57,58</sup>) after which the MIC structures become lower in energy.

To explain the icosahedral shell filling in Mg and Ca clusters Martin *et al.*<sup>60</sup> proposed the so-called *umbrella* model. According to this model enhanced stability is achieved each time a vertex and its five surrounding faces are covered (capping umbrellas). The capping umbrellas for MIC and TIC structures lead to different magic numbers. By covering of  $Ih_{13}$  the MIC umbrellas are completed at  $N = 19, 24, 28, 32, 36, 39, 43, 46, 49$  and  $55$ , whereas the TIC umbrellas give magic numbers for  $19, 23, 26, 29, 32$  and  $34$ . Comparing with our set of magic numbers (see above), we find that growth from  $Ni_{13}$  to  $Ni_{27}$  is icosahedral and it can be described according to the umbrella model. For  $N > 27$  our magic numbers coincide with the MIC magic figures. This confirms seemingly the suggestion<sup>11</sup> that at  $N = 27$  there is a transition from TIC to MIC growth. However, a detailed analysis of our structures shows that our structures for  $Ni_{28,1}$  and  $Ni_{32,1}$  are not icosahedral. Instead, the most stable icosahedral structure appears first at  $N = 35$  whereas the structures according to the MIC growth or to *fcc* packing is found up to  $N = 56$  with a single exception for  $N = 38$ . Thus the transition from anti-Mackay to Mackay covering occurs in the region of cluster sizes from  $28$  to  $34$ . Cluster growth in this range is complicated and there is a competition between icosahedral, polyicosahedral and tetrahedral structure. Probably this non-trivial growth was responsible for the difficulties in interpreting results of nitrogen-uptake experiments<sup>30,31,32</sup> for  $29 \leq N \leq 48$ .

At  $N = 55$  we have the next complete icosahedron. According to the TIC growth model we should then have magic number at  $N = 58, 61, 64, 67$ , and  $71$ ,<sup>11</sup> which is in excellent agreement with our results. At  $N = 71$  the TIC umbrella growth is completed. The MIC umbrella growth is completed at  $N = 71, 83, 92, 101, 110, 116, 125, 131$  and  $137$ , again in agreement with our calculated magic numbers.

Our study allows a more detailed analysis of possible growth processes that ultimately will confirm the complexity of the growth. Thus, in order to quantify whether the cluster of  $N$  atoms is related to that of  $N - 1$  atoms we consider first the structure of the lowest total



energy for the  $(N - 1)$ -cluster. For this we calculate and sort all interatomic distances,  $d_i$ ,  $i = 1, 2, \dots, \frac{N(N-1)}{2}$ . Subsequently we consider the  $N$  fragments of the  $N$ -cluster that can be obtained by removing one of the atoms and keeping the rest at their positions. For each of those we also calculate and sort all interatomic distances  $d'_i$ , and subsequently calculate

$$q = \left[ \frac{2}{N(N-1)} \sum_{i=1}^{N(N-1)/2} (d_i - d'_i)^2 \right]^{1/2}. \quad (9)$$

Of the  $N$  different values of  $q$  we choose the smallest one,  $q_{\min}$  and calculate the similarity function

$$S = \frac{1}{1 + q_{\min}/u_l} \quad (10)$$

( $u_l = 1 \text{ \AA}$ ) which approaches 1 if the  $\text{Ni}_N$  cluster is very similar to the  $\text{Ni}_{N-1}$  cluster plus an extra atom.

This function is shown in Fig. 11(a). We see indeed that for  $N$  up to around 40,  $S$  is significantly different from 1, giving support for the consensus that in this range the growth is complicated. For larger  $N$  we see again that around  $N \simeq 75$  some larger structural changes take place. Fig. 3 shows, however, that the energetically lowest isomers differ only little in energy. Therefore, one may ask whether isomers with a slightly higher energy play a role in the growth process. Accordingly, we examined whether the structure of the energetically lowest isomer of  $\text{Ni}_N$  would resemble any of the four energetically lowest isomers for  $\text{Ni}_{N-1}$  in the same sense as above, i.e., we use the quantity  $q$  in quantifying the structural difference. Out of the four different values for  $q$  (for the four different isomers) we choose the smallest one and construct the similarity function from this. The resulting function is shown in Fig. 11(b), and compared with Fig. 11(a) it is clearly seen that in particular in the region  $N > 50$  the similarity function now approaches 1, except for the clusters around  $N = 70-75$ , i.e., the region where we already in analysing other properties have found atypical behaviors. In Fig. 11(c) we show which of the four energetically lowest isomers of  $\text{Ni}_{N-1}$  leads to largest similarity with the  $\text{Ni}_N$  cluster, and from the fact that this only for the smaller  $N$  most often is the first isomer, we learn that the growth process is a complicated process where more different isomers are important, i.e., not only the energetically most stable one, although these may resemble each other (cf. Fig. 5). This means that it is difficult to imagine that the growth occurs as a one-by-one addition of atoms to the energetically most stable isomers.

## V. CONCLUSIONS

In summary, we have determined the four energetically lowest isomers of nickel clusters  $\text{Ni}_N$  in the range  $2 \leq N \leq 150$ , using a combination of the embedded-atom method in the version of Daw, Baskes and Foiles (for the calculation of the total energy for a given structure), the *variable metric/quasi-Newton* method (for the determination of the closest total-energy minimum), and our own *Aufbau/Abbau* method (for the determination of the global total-energy minimum). Although the calculations provide structural information for each individual cluster, separately,<sup>54</sup> that may be useful information for experimental studies, we have refrained from discussing these separately (some information is, however, given in the Appendix), but instead focused on identifying general trends for  $\text{Ni}_N$  clusters, and reducing the information on the individual clusters to some few key quantities like total energy (per atom), overall symmetry and shape, average bond length and coordination number, and similarity with other structures (*fcc* fragments, icosahedral clusters, or smaller clusters).

Since our total-energy approach (the embedded-atom method) has its roots in arguments for extended solids with delocalized atoms, we first verified that it could be applied also for the fairly open structures of our interest. We found that for the absolutely most ‘critical’ cases, i.e., the smallest clusters, our results are in excellent agreement with available theoretical and experimental information making us believe that our approach is accurate. Furthermore, we have also tried to use the parameterization of Voter and Chen<sup>61,62</sup> of the EAM, which has been produced in order to give accurate descriptions of also finite and more open systems, for some of the smallest clusters. To our satisfaction, no structural changes were found and, therefore, we did not pursue this approach.

Our study predicts a number of particularly stable clusters, i.e., magic numbers, which in many cases are in agreement with the prediction of other studies and in some cases with ‘common expectations’ although we stress that in our study they were found in a completely unbiased approach. These magic numbers were clearly visible both in the ‘stability function’ and in the total-energy difference between the energetically lowest and higher-lying isomers, whereas for the energetically higher-lying isomers, the differences in the total energy become small.

We found also that even for large values of  $N$  (above 2500) the total energy per atom

has still not converged to the bulk limit. Similarly, the average coordination number is for clusters with  $N$  around 150 still far from the bulk limit, whereas the average bond length has come close to the bulk limit for this size.

In order to study the structural properties we analysed the eigenvalues of the matrix containing the moments of inertia and introduced so-called similarity functions. The latter indicated that all the four isomers we have studied here are very similar in most cases, and that roughly spherical clusters were found mainly for the energetically lowest isomer but in some cases also for the second-lowest one, and that these often correspond to particularly stable structures. With the similarity functions we could identify clusters with a predominantly icosahedral structure and such with an essentially *fcc*-like structure. Whereas the former occurred for  $N$  around 13, 55, and 147, the latter was found, e.g., for  $N$  around 79. It was interesting to see that these structural motifs were built up over a larger range of  $N$  values and were, accordingly, not limited to those singular values of  $N$ .

By analysing the distribution of radial distances as a function of cluster size we could identify certain size regions, e.g.,  $N$  around 50, 75, 115, and above 140, where shell structures were clearly recognizable. This property, as well as several others, showed, furthermore, that all four isomers for a given  $N$  have very similar structures.

Chemical-probe experiments have been used in identifying the structure of the individual clusters, and for this we found an excellent agreement. Our study shows that for clusters with  $N$  around 50–60, a change occurs, so that above this size the number of  $N_2$  binding sites depends much weaker on  $N$  than below this size. This change is just on the boarder of the cluster sizes that have been studied experimentally and theoretically so far.

We used the magic numbers in analysing different models for cluster-growth processes. Generally, the cluster growth is according to multilayered-icosahedral or layer-by-layer growth. We found that the one-, two-, and three-shell Mackay icosahedra are the most stable structures for 13-, 55-, and 147-atom nickel clusters (the latter for the first time in unbiased studies). This result agrees well with the suggestion in Ref. 59 that Mackay icosahedra are the most stable structures up to  $N = 2300$ . But the cluster-growth pattern between two closed-shell icosahedra is not simple. It is predominantly icosahedral with islands of *fcc* growth for  $Ni_6$ ,  $Ni_{38}$ , tetrahedral for  $Ni_{28}$  and decahedral for  $Ni_{73}$ - $Ni_{79}$  and  $Ni_{104}$ . For  $14 \leq N \leq 27$  the growth is polyicosahedral. Moreover, we found a growth according to *hcp*/anti-Mackay for  $57 \leq N \leq 72$  and for  $148 \leq N \leq 150$ . From  $N = 35$  to  $N = 56$  (with

the exception of  $N = 38$ ) and from  $N = 80$  to  $N = 147$  (except for  $N = 104$ ) the MIC cluster growth was found. Thus, the change-over from the *hcp*-type of cluster growth to the *fcc* one always happens within a transition region of cluster sizes and not immediately.

Moreover, whereas the growth process only with difficulties could be identified for the smaller  $N$  (due to the lack of similarity between the clusters), for larger  $N$  we found that not only the energetically lowest isomers could be important in describing the growth. Thus, for all ranges of  $N$ , the growth is non-trivial.

A special case is that for  $N$  around 75. More different properties suggested that in this range special things occur. Analysing the total energy for different structures in this size range we found indeed that more structures were energetically close and, accordingly, would play a role for those clusters. Therefore, for these values of  $N$  there is a rapid and dramatic change in structure as a function of  $N$ .

## Acknowledgments

We gratefully acknowledge *Fonds der Chemischen Industrie* for very generous support. This work was supported by the SFB 277 of the University of Saarland. The authors are grateful to C. L. Cleveland, to Z. B. Güvenç and M. Büyükkata, and to K. Michaelian and I. L. Garzón for providing us with the coordinates of some cluster structures. We would like to thank J. P. K. Doye for references to some recent studies on nickel clusters.

## APPENDIX A: STRUCTURE OF THE CLUSTERS

In this appendix we shall present the structure of some of the clusters without entering a detailed discussion of each clusters individually. We shall use the notation  $N.k$  for the  $Ni_N$  cluster of the  $k$ -lowest total energy. We add that the nuclear coordinates and total energies for the optimized clusters can be obtained from the authors upon request.

3.1: equilateral triangle. 4.1: tetrahedron. 5.1 trigonal bipyramid. 6.1 octahedron. 6.2: pentagonal bipyramid without a single pentagonal vertex. 7.1: pentagonal bipyramid. 7.2: capped octahedron. 8.1: bisdisphenoid. 8.2: capped pentagonal bipyramid. 9.1: bicapped pentagonal bipyramid. 9.2: tricapped trigonal prism. 10.1: tricapped pentagonal bipyramid. 10.2: trapezoidal antiprism. 11.1: quadricapped pentagonal bipyramid. 11.2:

two pentagonal bipyramids with a common face. 12.1: icosahedron without one atom at one vertex. 12.2: low symmetry. 12.3: trapezoidal bipyramid with capped trigonal faces. 12.4: truncated trigonal bipyramid. 13.1: Mackay icosahedron. 13.2, 13.3, 13.4: similar structures as 13.1, but with the move of a vertex atom to a face. 14.1: the structure of 13.1 with the capping of one of the trigonal faces. 14.2: similar, but with the 14th atom on the top of a pentagonal edge. 14.3: bicapped hexagonal antiprism. 14.4: tricapped pentagonal prism. 15.1: bicapped icosahedron. 15.2: centered bicapped hexagonal antiprism. 15.3, 15.4: capped pentagonal prism.

16.1: tricapped icosahedron. 18.1: double icosahedra without one atom in one pentagonal ring. 18.2: double icosahedra without one atom in a capping vertex. 19.1: double icosahedron. 19.2, 19.3, 19.4: derivatives of the double icosahedron by moving of an atom from an apex or from a pentagonal ring to a face-capped or a bridging position. 20.1: double icosahedron with an atom added to the a pentagon in a bridging position. 21.1, 21.2, 21.3, 21.4: derivatives of the double icosahedron with two additional atoms at bridging or capping positions. 22.1, 22.2: triple icosahedron without one atom either from a pentagonal ring (22.1) or from a capping position (22.2). 23.1: triple icosahedron. 24.1, 24.2: triple icosahedron with an additional atom. 25.1: three sequentially interpenetrating icosahedra whose vertices are located on one line. 26.1: six interpenetrating double icosahedra (a polyicosahedron). 27.1: the polyicosahedron plus an extra atom at a pentagonal cap. 28.1: tetrahedron.

In general, the structures for  $29 \leq N \leq 34$  do not display any dominant morphology — there is a competition between tetrahedral, polyicosahedral, and icosahedral packings. One can consider this size range as a transition range from *hcp* to *fcc* growth.

29.1: distorted tetrahedron. 30.1: a polyicosahedral morphology. 32.1: derived from the 28.1 tetrahedron by adding four surface atoms. 35.1: MIC/Mackay structure. 36.1, 37.1: contain icosahedral motifs. 38.1: truncated octahedron. 38.2, 38.3: icosahedral fragments. 39.1: the second Mackay icosahedron (55.1) without a 16-atom cap. 39.4: a *fcc* cluster.

49.1: the second Mackay icosahedron (55.1) without one face. 51.1, 52.1, 53.1, 54.1: obtained from 49.1 by adding atom by atom until 55.1: second Mackay icosahedron. 54.2: as 55.1 but without the central atom. 56.1: as 55.1 but with an extra atom at the center of a triangular face.  $N = 56 - 71$ : TIC/anti-Mackay growth in accordance with the umbrella model.

75.1: (2,2,2) Marks decahedron. 79.2: a *fcc* cluster. 104.1: related (2,3,2) Marks decahe-

dron. 147.1: three-layer icosahedron.

---

- <sup>1</sup> C. J. Tsai and K. D. Jordan, J. Phys. Chem. **97**, 11227 (1993).
- <sup>2</sup> M. Calleja, C. Rey, M. M. G. Alemany, L. J. Gallego, P. Ordejón, D. Sánchez-Portal, E. Artacho and J. M. Soler, Phys. Rev. B **60**, 2020 (1999).
- <sup>3</sup> M. C. Michelini, R. Pis Diez, and A. H. Jubert, Int. J. Quant. Chem. **85**, 22 (2001).
- <sup>4</sup> F. A. Reuse and S. N. Khanna, Chem. Phys. Lett. **234**, 77 (1995).
- <sup>5</sup> S. K. Nayak, B. Reddy, B. K. Rao, S. N. Khanna, and P. Jena, Chem. Phys. Lett. **253**, 390 (1996).
- <sup>6</sup> N. Desmarais, C. Jamorski, F. A. Reuse, and S. N. Khanna, Chem. Phys. Lett. **294**, 480 (1998).
- <sup>7</sup> S. Krüger, T. J. Seemüller, A. Wörndle, and N. Rösch, Int. J. Quant. Chem. **80**, 567 (2000).
- <sup>8</sup> D. G. Vlachos, L. D. Schmidt, and R. Aris, J. Chem. Phys. **96**, 6880 (1992).
- <sup>9</sup> C. Rey, L. J. Gallego, J. García-Rodeja, J. A. Alonso and M. P. Iñiguez, Phys. Rev. B **48**, 8253 (1993).
- <sup>10</sup> J. M. Montejano-Carrizales, M. P. Iñiguez, and J. A. Alonso, J. Cluster. Sci. **5**, 287 (1994).
- <sup>11</sup> J. M. Montejano-Carrizales, M. P. Iñiguez, J. A. Alonso, and M. J. López, Phys. Rev. B **54**, 5961 (1996).
- <sup>12</sup> L. García González and J. M. Montejano-Carrizales, phys. stat. sol. **220**, 357 (2000).
- <sup>13</sup> Z. B. Güvenç, J. Jellinek and A. F. Voter, in *Physics and Chemistry of Finite systems: From Clusters to Crystals*, edited by P. Jena, S. N. Khanna and B. K. Rao (Kluwer, Dordrecht, 1992), Vol I, p. 411.
- <sup>14</sup> Z. B. Güvenç and J. Jellinek, Z. Phys. D **26**, 304 (1993).
- <sup>15</sup> M. Büyükkata, Z. B. Güvenç, S. Özçelik, P. Durmus, and J. Jellinek, Int. J. Quant. Chem. **84**, 208 (2001).
- <sup>16</sup> M. S. Stave and A. E. DePristo, J. Chem. Phys. **97**, 3386 (1992).
- <sup>17</sup> T. L. Wetzel and A. E. DePristo, J. Chem. Phys. **105**, 572 (1996).
- <sup>18</sup> J. Jellinek and I. L. Garzón, Z. Phys. D **20**, 239 (1991).
- <sup>19</sup> I. L. Garzón and J. Jellinek, in *Physics and Chemistry of Finite systems: From Clusters to Crystals*, ed. P. Jena, S.N. Khanna and B.K. Rao, Kluwer, Dordrecht, 1992, Vol I, p. 405.
- <sup>20</sup> M. J. Lopez and J. Jellinek, Phys. Rev. A **50**, 1445 (1994).

- <sup>21</sup> F. Aguilera-Granja, S. Bouarab, M. J. López, A. Vega, J. M. Montejano-Carrizales, M. P. Iñiguez, and J. A. Alonso, Phys. Rev. B **57**, 12469 (1998).
- <sup>22</sup> K. Michaelian, N. Rendón, and I. L. Garzón, Phys. Rev. B **60**, 2000 (1999).
- <sup>23</sup> J. P. K. Doye and D. J. Wales, New J. Chem. **22**, 733 (1998).
- <sup>24</sup> J. A. Northby, J. Chem. Phys. **87**, 6166 (1987).
- <sup>25</sup> S. K. Nayak, S. N. Khanna, B. K. Rao, and P. Jena, J. Chem. Phys. A **101**, 1072 (1997).
- <sup>26</sup> L. D. Lloyd, R. L. Johnston, J. Chem. Soc., Dalton Trans. **3**, 307 (2000).
- <sup>27</sup> W. Hu, L. M. Mei, and H. Li, Solid State Commun. **100**, 129 (1996).
- <sup>28</sup> N. N. Lathiotakis, A. N. Andriotis, M. Menon and J. Connolly, J. Chem. Phys. **104**, 992 (1996).
- <sup>29</sup> E. K. Parks, B. J. Winter, T. D. Klots and S. J. Riley, J. Chem. Phys. **94**, 1882 (1991).
- <sup>30</sup> E. K. Parks, L. Zhu, J. Ho and S. J. Riley, J. Chem. Phys. **100**, 7206 (1994).
- <sup>31</sup> E. K. Parks, L. Zhu, J. Ho and S. J. Riley, J. Chem. Phys. **102**, 7377 (1995).
- <sup>32</sup> E. K. Parks and S. J. Riley Z. Phys. D. **33**, 59, (1995).
- <sup>33</sup> E. K. Parks, G. C. Nieman, K. P. Kerns, and S. J. Riley, J. Chem. Phys. **107**, 1861 (1997).
- <sup>34</sup> E. K. Parks, K. P. Kerns, and S. J. Riley, J. Chem. Phys. **109**, 10207 (1998).
- <sup>35</sup> E. K. Parks, K. P. Kerns, and S. J. Riley, J. Chem. Phys. **114**, 2228 (2001).
- <sup>36</sup> M. B. Knickelbein, J. Chem. Phys. **115**, 5957 (2001).
- <sup>37</sup> M. Pellarin, B. Baguenard, J. L. Vialle, J. Lerme, M. Broyer, J. Miller and A. Perez, Chem. Phys. Lett. **217**, 349 (1994).
- <sup>38</sup> V. G. Grigoryan and M. Springborg, Phys. Chem. Chem. Phys. **3**, 5125 (2001).
- <sup>39</sup> V. G. Grigoryan and M. Springborg, Chem. Phys. Lett. **375**, 219 (2003).
- <sup>40</sup> M. S. Daw and M. I. Baskes, Phys. Rev. Lett. **50**, 1285 (1983).
- <sup>41</sup> M. S. Daw and M. I. Baskes, Phys. Rev. B **29**, 6443 (1984).
- <sup>42</sup> S. M. Foiles, M. S. Daw and M. I. Baskes, Phys. Rev. B **33**, 7983 (1986).
- <sup>43</sup> M. S. Daw, S. M. Foiles and M. I. Baskes, Mat. Sci. Rep. **9**, 251 (1993).
- <sup>44</sup> E. Clementi and C. Roetti, At. Data Nucl. Data Tables **14**, 177 (1974).
- <sup>45</sup> A.D. McLean and R.S. McLean, At. Data Nucl. Data Tables **26**, 197 (1981).
- <sup>46</sup> J.H. Rose, J.R. Smith, F. Guinea and J. Ferrante, Phys. Rev. B **29**, 2963 (1984).
- <sup>47</sup> Internet address: 146.246.250.1
- <sup>48</sup> W. H. Press, S. A. Teukolsky, W. T. Vetterling, B. P. Flannery, in *Numerical Recipes in FORTRAN: the Art of Scientific Computing*, (Cambridge University Press, Cambridge, 1992), p.

- <sup>49</sup> D. J. Wales and J. P. K. Doye, J. Phys. Chem. A **101**, 5111 (1997).
- <sup>50</sup> J. C. Pinegar, J. D. Langenberg, C. A. Arrington, E. M. Spain, and M. D. Morse, J. Chem. Phys. **102**, 666 (1995).
- <sup>51</sup> Z. B. Güvenç and M. Büyükkata (private communication).
- <sup>52</sup> E. Curotto, A. Matro, D. L. Freeman, and J. D. Doll, J. Chem. Phys. **108**, 729 (1998).
- <sup>53</sup> C. Rey, J. García-Rodeja and L.J. Gallego, Phys. Rev. B **54**, 2942 (1996).
- <sup>54</sup> V. G. Grigoryan and M. Springborg, unpublished results that can be obtained upon request from the authors.
- <sup>55</sup> J. A. Alonso, Chem. Rev. **100**, 637 (2000).
- <sup>56</sup> J. P. K. Doye, D. J. Wales, and R. S. Berry, J. Chem. Phys. **103**, 4234 (1995).
- <sup>57</sup> I. A. Harris, R. S. Kidwell, and J. A. Northby, Phys. Rev. Lett. **53**, 2390 (1984).
- <sup>58</sup> M. W. Sung, R. Kawai, and J. H. Weare, Phys. Rev. Lett. **73**, 3552 (1994).
- <sup>59</sup> C. L. Cleveland and U. Landman, J. Chem. Phys. **94**, 7376 (1991).
- <sup>60</sup> T. P. Martin, T. Bergmann, H. Gölich, and T. Lange, Chem. Phys. Lett. **176**, 343 (1991).
- <sup>61</sup> A. F. Voter and S. P. Chen, in *Characterization of Defects in Materials*, edited by R. W. Siegal, J. R. Weertman, and R. Sinclair, MRS Symposia Proceedings No. 82 (Materials Research Society, Pittsburgh, 1987), p. 175.
- <sup>62</sup> A. F. Voter, in *Intermetallic Compounds*, edited by J. H. Westbrook and R. L. Fleischer (John Wiley and Sons, Ltd, 1995), Vol. 1, p. 77.



TABLE I: The symmetry (Sym.) and averaged bond length ( $\langle r \rangle$ ) for smaller  $\text{Ni}_N$  clusters from different experimental and theoretical studies. EAM, TBMD, FS, SC, AI, EMT,  $n\text{G}$ , and exp denotes Embedded-Atom calculations, tight-binding molecular-dynamics calculations, Finnis-Sinclair potential, Sutton-Chen potential, *ab initio* calculations, effective-medium-theory calculations, many-body Gupta potential, and experiment, respectively. For some values of  $N$ , more different metastable isomers have been found, and they have then been characterized by an additional number (e.g., 7.1, 7.2, 7.3, and 7.4, with 7.1 being the stabler one, 7.2 the second-most stable one, a.s.o.)

$N$	Ref.	Sym.	$\langle r \rangle$ (Å)	Method	$N$	Ref.	Sym.	$\langle r \rangle$ (Å)	Method	$N$	Ref.	Sym.	$\langle r \rangle$ (Å)	Method	
2	here	D <sub>∞h</sub>	2.12	EAM	23		O <sub>h</sub>	–	SC	23		D <sub>2d</sub>	–	SC	
	28	D <sub>∞h</sub>	2.20	TBMD	20,22		O <sub>h</sub>	–	$n$ G	20		D <sub>2d</sub>	–	$n$ G	
	25	D <sub>∞h</sub>	2.01	FS	3	C <sub>i</sub> (∼O <sub>h</sub> )	2.40	AI		3		T <sub>d</sub>	2.32	AI	
	3	D <sub>∞h</sub>	2.13	AI	4		D <sub>4h</sub>	2.33	AI	4		O <sub>h</sub>	2.16	AI	
	4	D <sub>∞h</sub>	1.99	AI	30		O <sub>h</sub>	–	exp	6	D <sub>2</sub> (∼D <sub>2d</sub> )	2.28	AI		
	2	D <sub>∞h</sub>	2.17	AI	6.2	here	C <sub>2v</sub>	2.37	EAM	7		D <sub>2d</sub>	2.37	AI	
	50	D <sub>∞h</sub>	2.15	exp	22		C <sub>2v</sub>	–	$n$ G	30		D <sub>2d</sub>	–	exp	
3	here	D <sub>3h</sub>	2.25	EAM	3		D <sub>2h</sub>	2.40	AI	8.2	here	C <sub>s</sub>	2.40	EAM	
	28	D <sub>3h</sub>	2.30	TBMD	7.1	here	D <sub>5h</sub>	2.39	EAM	51		C <sub>s</sub>	2.38	EAM	
	25	D <sub>3h</sub>	2.10	FS	28		D <sub>5h</sub>	2.51	TBMD	16		C <sub>s</sub>	–	EMT	
	23	D <sub>3h</sub>	–	SC	25		D <sub>5h</sub>	2.28	FS	6		C <sub>s</sub>	2.28	AI	
	20	D <sub>3h</sub>	–	$n$ G	15,51		D <sub>5h</sub>	2.37	EAM	7		C <sub>2v</sub>	2.36	AI	
	3	D <sub>3h</sub>	2.26	AI	16		D <sub>5h</sub>	–	EMT	30		C <sub>s</sub>	–	exp	
	4	C <sub>2v</sub>	2.15	AI	23		D <sub>5h</sub>	–	SC	8.3	here	D <sub>3d</sub>	2.39	EAM	
	30	D <sub>3h</sub>	–	exp	20,22		D <sub>5h</sub>	–	$n$ G	51		D <sub>3d</sub>	2.36	EAM	
4	here	T <sub>d</sub>	2.32	EAM	6		C <sub>3v</sub>	2.27	AI	6		C <sub>2v</sub>	2.26	AI	
	28	D <sub>4h</sub>	2.26	TBMD	5		C <sub>3v</sub>	–	AI	7	D <sub>3d</sub> /C <sub>s</sub>	2.37/2.38	AI		
	25	T <sub>d</sub>	2.20	FS	30		C <sub>3v</sub>	–	exp	8.4	here	C <sub>2v</sub>	2.39	EAM	
	16	T <sub>d</sub>	–	EMT	7.2	here	C <sub>3v</sub>	2.38	EAM	51		C <sub>2v</sub>	2.36	EAM	
	23	T <sub>d</sub>	–	SC	51		C <sub>3v</sub>	2.36	EAM	6		D <sub>2d</sub>	2.31	AI	
	20	T <sub>d</sub>	–	$n$ G	16		C <sub>3v</sub>	–	EMT	13.1	here	I <sub>h</sub>	2.36/2.48	EAM	
	3	D <sub>2d</sub> (∼T <sub>d</sub> )	2.33	AI	22		C <sub>3v</sub>	–	$n$ G	28		I <sub>h</sub>	2.57	TBMD	
	4	D <sub>2d</sub> /D <sub>4h</sub>	2.17/2.10	AI	6	C <sub>2v</sub> (∼D <sub>5h</sub> )	2.28	AI		25		I <sub>h</sub>	–/2.39	FS	
	30	–	–	exp	5		D <sub>5h</sub>	–	AI	15,53		I <sub>h</sub>	–	EAM	
	5	here	D <sub>3h</sub>	2.35	EAM	30		D <sub>5h</sub>	–	exp	20,22		I <sub>h</sub>	–	$n$ G
	28	T <sub>d</sub>	2.42	TBMD	7.3	here	C <sub>2</sub>	2.38	EAM	16		I <sub>h</sub>	–	EMT	
	25	D <sub>3h</sub>	2.23	FS	51		C <sub>3v</sub>	2.36	EAM	23		I <sub>h</sub>	–	SC	
	16	D <sub>3h</sub>	–	EMT	16		C <sub>2</sub>	–	EMT	4		I <sub>h</sub>	2.23/2.34	AI	
	23	D <sub>3h</sub>	–	SC	22		C <sub>2</sub>	–	$n$ G	2		I <sub>h</sub>	2.41/2.53	AI	
	20	D <sub>3h</sub>	–	$n$ G	6		C <sub>3v</sub>	2.28	AI	30		I <sub>h</sub>	–	exp	
	3	C <sub>4v</sub>	2.35	AI	7.4	here	C <sub>3v</sub>	2.39	EAM	13.2	here	C <sub>s</sub>	2.44	EAM	
	4	D <sub>3h</sub>	2.25	AI	51		C <sub>2</sub>	2.37	EAM	28		O <sub>h</sub>	2.48	TBMD	
	30	D <sub>3h</sub>	–	exp	6		C <sub>2v</sub>	2.25	AI	16		D <sub>3h</sub>	–	EMT	
6.1	here	O <sub>h</sub>	2.36	EAM	8.1	here	D <sub>2d</sub>	2.38	EAM	22		C <sub>s</sub>	–	$n$ G	
	28	D <sub>4h</sub>	2.47	TBMD	15,51		D <sub>2d</sub>	2.36	EAM	13.3	here	C <sub>s</sub>	2.44	EAM	
	25	O <sub>h</sub>	2.25	FS	28		C <sub>2h</sub>	2.50	TBMD	16		O <sub>h</sub>	–	EMT	
	16	O <sub>h</sub>	–	EMT	25	D <sub>2d</sub> <sup>25</sup>	2.25	FS		22		C <sub>s</sub>	–	$n$ G	
					16		D <sub>2d</sub>	–	EMT	here		C <sub>s</sub>	2.43	EAM	

TABLE II: Point groups of the optimized clusters.

$N$	$N.1$	$N.2$	$N.3$	$N.4$	$N$	$N.1$	$N.2$	$N.3$	$N.4$	$N$	$N.1$	$N.2$	$N.3$	$N.4$	$N$	$N.1$	$N.2$	$N.3$	$N.4$
2	$D_{\infty h}$				40	$C_s$	$C_s$	$C_1$	$C_2$	78	$C_1$	$C_1$	$C_s$	$C_s$	116	$C_{5v}$	$C_1$	$C_1$	$C_1$
3	$D_{3h}$				41	$C_s$	$C_s$	$C_1$	$C_1$	79	$C_{2v}$	$O_h$	$D_{3h}$	$C_1$	117	$C_1$	$C_s$	$C_1$	$C_1$
4	$T_d$				42	$C_s$	$C_s$	$C_1$	$C_s$	80	$C_1$	$C_s$	$C_{2v}$	$C_s$	118	$C_s$	$C_s$	$C_1$	$C_1$
5	$D_{3h}$				43	$C_s$	$C_s$	$C_1$	$C_s$	81	$C_2$	$C_s$	$C_s$	$C_{2v}$	119	$C_s$	$C_1$	$C_1$	$C_1$
6	$O_h$	$C_{2v}$			44	$C_1$	$C_s$	$C_1$	$C_s$	82	$C_1$	$C_s$	$C_s$	$C_1$	120	$C_1$	$C_1$	$C_1$	$C_s$
7	$D_{5h}$	$C_{3v}$	$C_2$	$C_{3v}$	45	$C_s$	$C_s$	$C_1$	$C_1$	83	$C_{2v}$	$D_3$	$C_2$	$C_s$	121	$C_1$	$C_1$	$C_1$	$C_1$
8	$D_{2d}$	$C_s$	$D_{3d}$	$C_{2v}$	46	$C_{2v}$	$C_1$	$C_1$	$C_1$	84	$C_s$	$C_1$	$C_1$	$C_1$	122	$C_1$	$C_1$	$C_s$	$C_1$
9	$C_{2v}$	$D_{3h}$	$C_{2v}$	$C_s$	47	$C_1$	$C_s$	$C_s$	$C_s$	85	$C_1$	$C_s$	$C_1$	$C_1$	123	$C_s$	$C_s$	$C_1$	$C_1$
10	$C_{3v}$	$D_{2h}$	$C_2$	$C_{2v}$	48	$C_s$	$C_s$	$C_s$	$C_1$	86	$C_3$	$C_s$	$C_1$	$C_1$	124	$C_s$	$C_s$	$C_s$	$C_1$
11	$C_{2v}$	$C_2$	$C_{2v}$	$C_2$	49	$C_{3v}$	$C_1$	$C_s$	$C_s$	87	$C_1$	$C_1$	$C_s$	$C_s$	125	$C_s$	$C_1$	$C_1$	$C_1$
12	$C_{5v}$	$C_1$	$D_{2d}$	$D_{3h}$	50	$C_s$	$C_s$	$C_{2v}$	$C_s$	88	$C_s$	$C_s$	$C_s$	$C_1$	126	$C_s$	$C_s$	$C_s$	$C_1$
13	$I_h$	$C_s$	$C_s$	$C_s$	51	$C_{2v}$	$C_s$	$C_s$	$C_2$	89	$C_{3v}$	$C_s$	$C_1$	$C_s$	127	$C_{2v}$	$C_s$	$C_1$	$C_1$
14	$C_{3v}$	$C_{2v}$	$C_s$	$C_{2v}$	52	$C_{3v}$	$C_s$	$C_s$	$C_s$	90	$C_s$	$C_1$	$C_s$	$C_1$	128	$C_1$	$C_1$	$C_s$	$C_s$
15	$C_{2v}$	$D_{6d}$	$C_{2v}$	$C_{2v}$	53	$C_{2v}$	$D_{5d}$	$C_{2v}$	$C_s$	91	$C_s$	$C_s$	$C_s$	$C_1$	129	$C_s$	$C_s$	$C_s$	$C_2$
16	$C_s$	$C_s$	$C_2$	$D_{3h}$	54	$C_{5v}$	$I_h$	$C_{2v}$	$C_s$	92	$C_{3v}$	$T$	$C_1$	$C_1$	130	$C_1$	$C_s$	$C_s$	$C_1$
17	$C_2$	$C_s$	$C_s$	$C_{3v}$	55	$I_h$	$C_s$	$C_s$	$C_s$	93	$C_1$	$C_1$	$C_1$	$C_1$	131	$C_{2v}$	$C_1$	$C_1$	$C_1$
18	$C_s$	$C_{5v}$	$C_s$	$C_1$	56	$C_{3v}$	$C_{3v}$	$C_s$	$C_1$	94	$C_1$	$C_1$	$C_1$	$C_1$	132	$C_1$	$C_1$	$C_s$	$C_1$
19	$D_{5h}$	$C_1$	$C_s$	$C_1$	57	$C_s$	$C_s$	$C_s$	$C_s$	95	$C_1$	$C_3$	$C_1$	$C_1$	133	$C_1$	$C_s$	$C_s$	$C_1$
20	$C_{2v}$	$D_{3d}$	$D_2$	$D_2$	58	$C_{3v}$	$C_s$	$C_1$	$C_1$	96	$C_1$	$C_1$	$C_1$	$C_{2v}$	134	$C_{3v}$	$C_s$	$C_1$	$C_1$
21	$C_1$	$C_{2v}$	$C_{2v}$	$C_s$	59	$C_{2v}$	$C_1$	$C_1$	$C_{2v}$	97	$C_1$	$C_1$	$C_1$	$C_{2v}$	135	$C_s$	$C_1$	$C_s$	$C_s$
22	$C_s$	$C_s$	$C_1$	$C_s$	60	$C_s$	$C_s$	$C_s$	$C_1$	98	$C_s$	$C_s$	$C_s$	$C_s$	136	$C_s$	$C_s$	$C_s$	$C_1$
23	$D_{3h}$	$C_2$	$C_s$	$C_1$	61	$C_{2v}$	$C_s$	$C_s$	$C_1$	99	$C_{2v}$	$C_1$	$C_s$	$C_s$	137	$C_{3v}$	$C_{2v}$	$C_{2v}$	$C_1$
24	$C_{2v}$	$C_s$	$D_3$	$C_s$	62	$C_{2v}$	$C_s$	$C_1$	$C_1$	100	$C_s$	$C_s$	$C_{5v}$	$C_1$	138	$C_{3v}$	$C_s$	$C_1$	$C_s$
25	$C_{2v}$	$C_3$	$D_{5d}$	$C_s$	63	$C_1$	$C_s$	$C_1$	$C_s$	101	$C_{2v}$	$D_{5h}$	$C_s$	$C_1$	139	$C_{2v}$	$C_s$	$C_s$	$C_s$
26	$T_d$	$C_s$	$C_1$	$C_s$	64	$C_s$	$C_1$	$C_1$	$C_{2v}$	102	$C_s$	$C_1$	$C_1$	$C_{2v}$	140	$C_s$	$C_s$	$C_1$	$C_s$
27	$C_{2v}$	$C_s$	$C_s$	$C_s$	65	$C_1$	$C_2$	$C_1$	$C_1$	103	$C_1$	$C_s$	$C_1$	$C_1$	141	$C_{5v}$	$C_{3v}$	$C_2$	$C_1$
28	$T$	$D_2$	$C_{3v}$	$C_s$	66	$C_1$	$C_1$	$C_1$	$C_1$	104	$C_{2v}$	$C_1$	$C_s$	$C_1$	142	$C_s$	$C_s$	$C_{5v}$	$C_s$
29	$C_3$	$D_{3h}$	$C_{2v}$	$C_s$	67	$C_2$	$C_s$	$C_{2v}$	$C_s$	105	$C_1$	$C_1$	$C_1$	$C_s$	143	$C_{2v}$	$C_s$	$C_s$	$C_s$
30	$C_{2v}$	$C_s$	$C_1$	$C_1$	68	$C_1$	$C_1$	$C_1$	$C_2$	106	$C_1$	$C_1$	$C_1$	$C_1$	144	$C_{3v}$	$C_s$	$C_s$	$C_s$
31	$C_s$	$C_3$	$C_s$	$C_1$	69	$C_1$	$C_1$	$C_{5v}$	$C_1$	107	$C_s$	$C_1$	$C_1$	$C_s$	145	$C_{2v}$	$C_{2v}$	$D_{5d}$	$C_s$
32	$D_3$	$C_{2v}$	$C_{2v}$	$C_s$	70	$C_{5v}$	$C_1$	$C_5$	$C_5$	108	$C_s$	$C_1$	$C_1$	$C_1$	146	$C_{5v}$	$C_s$	$C_s$	$C_s$
33	$C_2$	$C_s$	$C_s$	$C_s$	71	$C_5$	$C_{5v}$	$C_{2v}$	$C_s$	109	$C_1$	$C_s$	$C_1$	$C_1$	147	$I_h$	$C_1$	$C_1$	$C_1$
34	$C_s$	$C_s$	$C_s$	$C_1$	72	$C_s$	$C_s$	$C_s$	$C_1$	110	$C_s$	$C_s$	$C_1$	$C_1$	148	$C_s$	$C_s$	$C_s$	$C_1$
35	$C_{2v}$	$D_3$	$D_3$	$C_s$	73	$C_s$	$C_s$	$C_s$	$C_1$	111	$C_s$	$C_s$	$C_1$	$C_1$	149	$C_s$	$C_s$	$C_s$	$C_1$
36	$C_s$	$C_1$	$C_1$	$C_1$	74	$C_{5v}$	$C_s$	$C_1$	$C_1$	112	$C_s$	$C_1$	$C_s$	$C_1$	150	$C_{3v}$	$C_{3v}$	$C_s$	$C_1$
37	$C_2$	$C_1$	$C_1$	$C_1$	75	$D_{5h}$	$C_s$	$C_s$	$C_s$	113	$C_s$	$C_s$	$C_1$	$C_1$					
38	$O_h$	$C_{5v}$	$C_{5v}$	$C_1$	76	$C_s$	$C_{2v}$	$C_s$	$C_1$	114	$C_s$	$C_s$	$C_{5v}$	$C_1$					
39	$C_{5v}$	$C_5$	$C_s$	$C_{4v}$	77	$C_{2v}$	$C_2$	$C_s$	$C_2$	115	$C_{5v}$	$C_s$	$C_{5v}$	$C_1$					

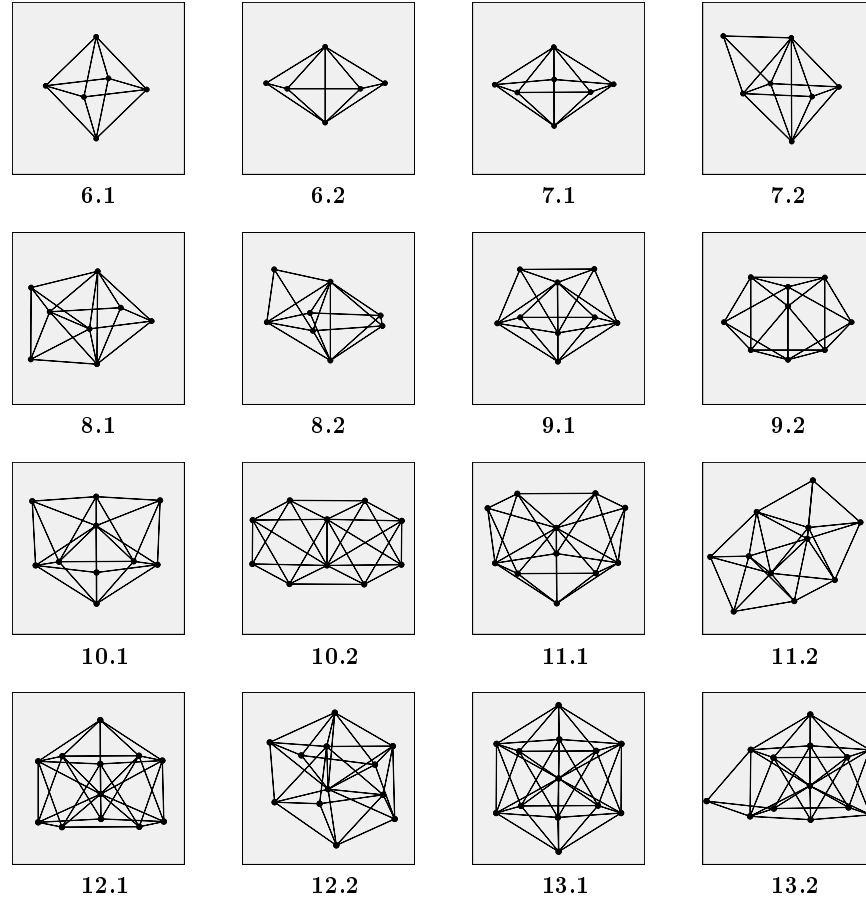


FIG. 1: The optimized geometries of the two energetically lowest isomers of  $\text{Ni}_N$  clusters for  $6 \leq N \leq 13$

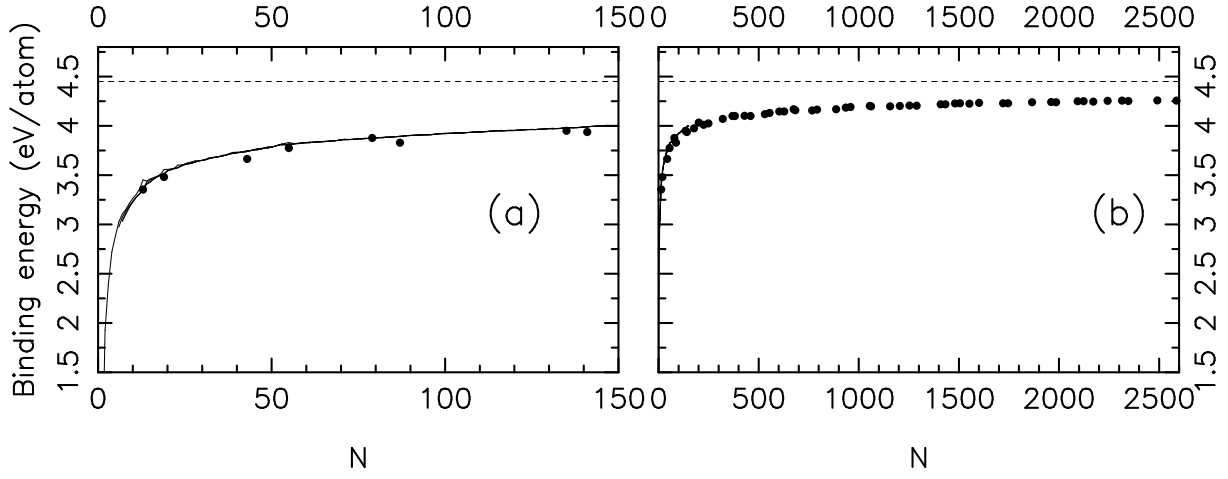


FIG. 2: Binding energy per atom as a function of size for the four energetically lowest isomers for  $N$  up to 150 (continuous curves) together with that of relaxed, spherical parts of the *fcc* crystal structure with an atom at the center (closed circles). The horizontal dashed lines mark the value for bulk Ni as obtained with the same method.

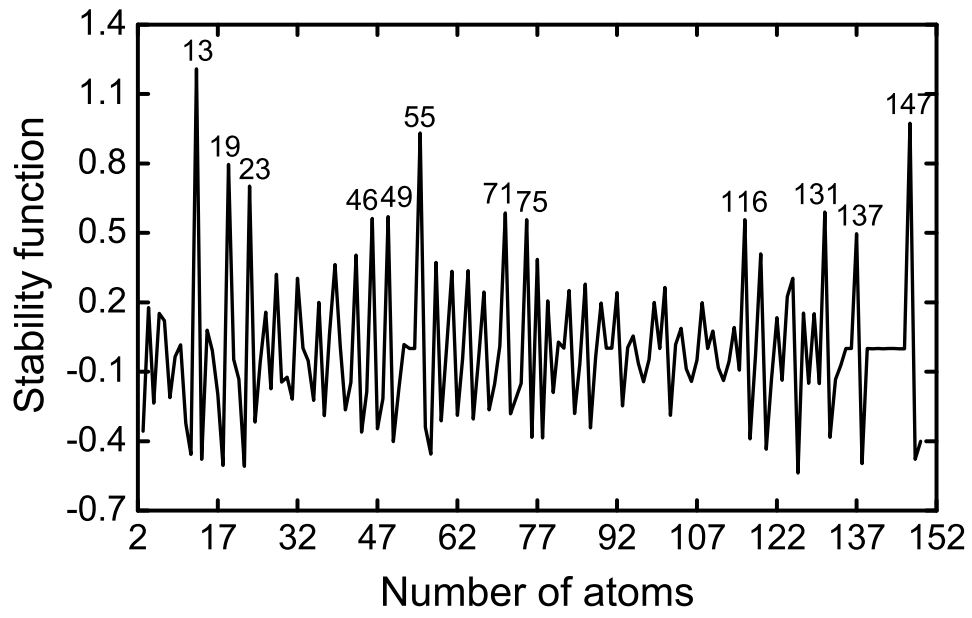


FIG. 3: The stability function as a function of cluster size.

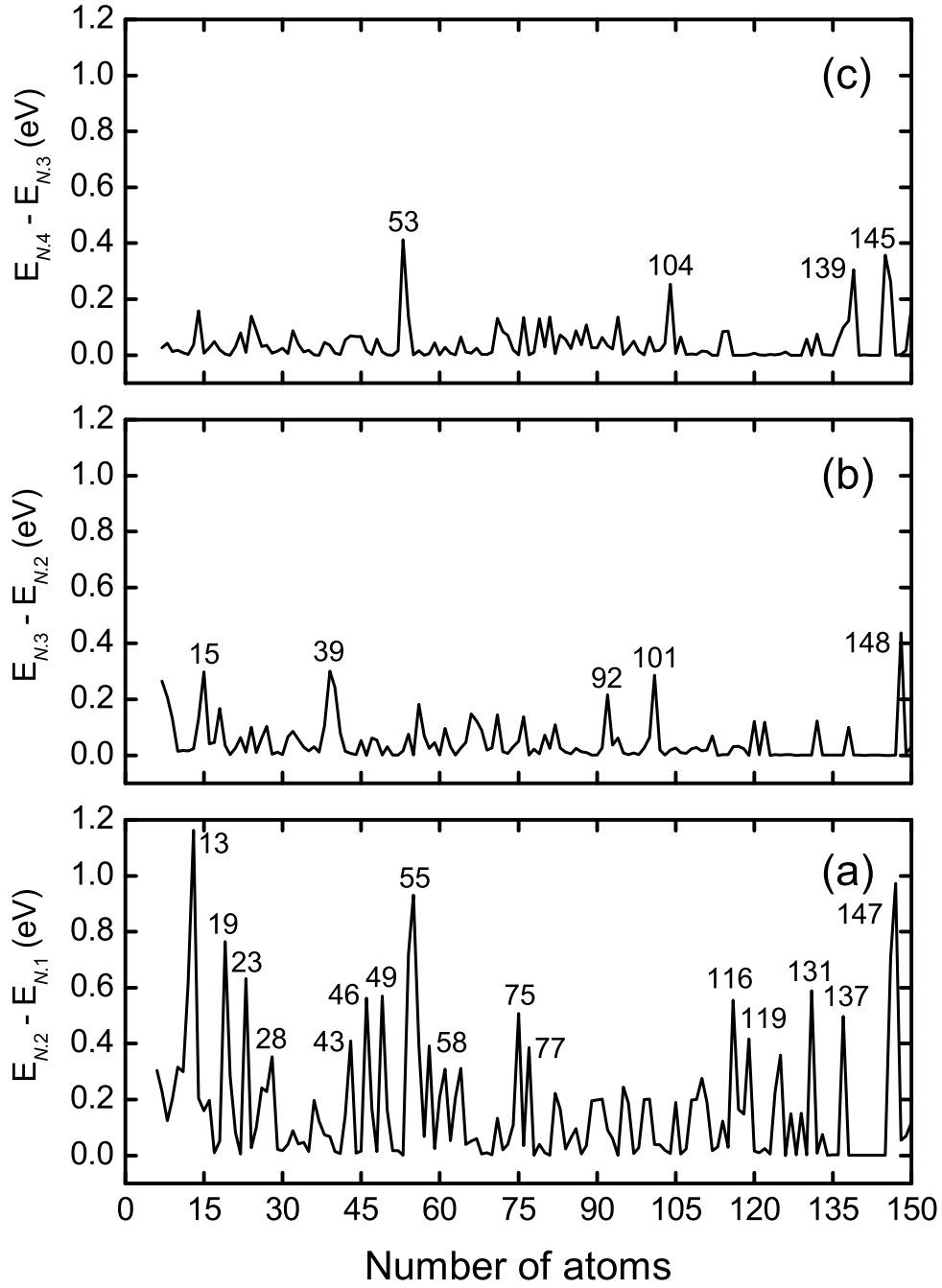


FIG. 4: The total-energy difference between the two energetically neighboring isomers as a function of cluster size. (a) shows the difference between the second and the first, (b) between the third and the second and (c) between fourth and the third isomer.

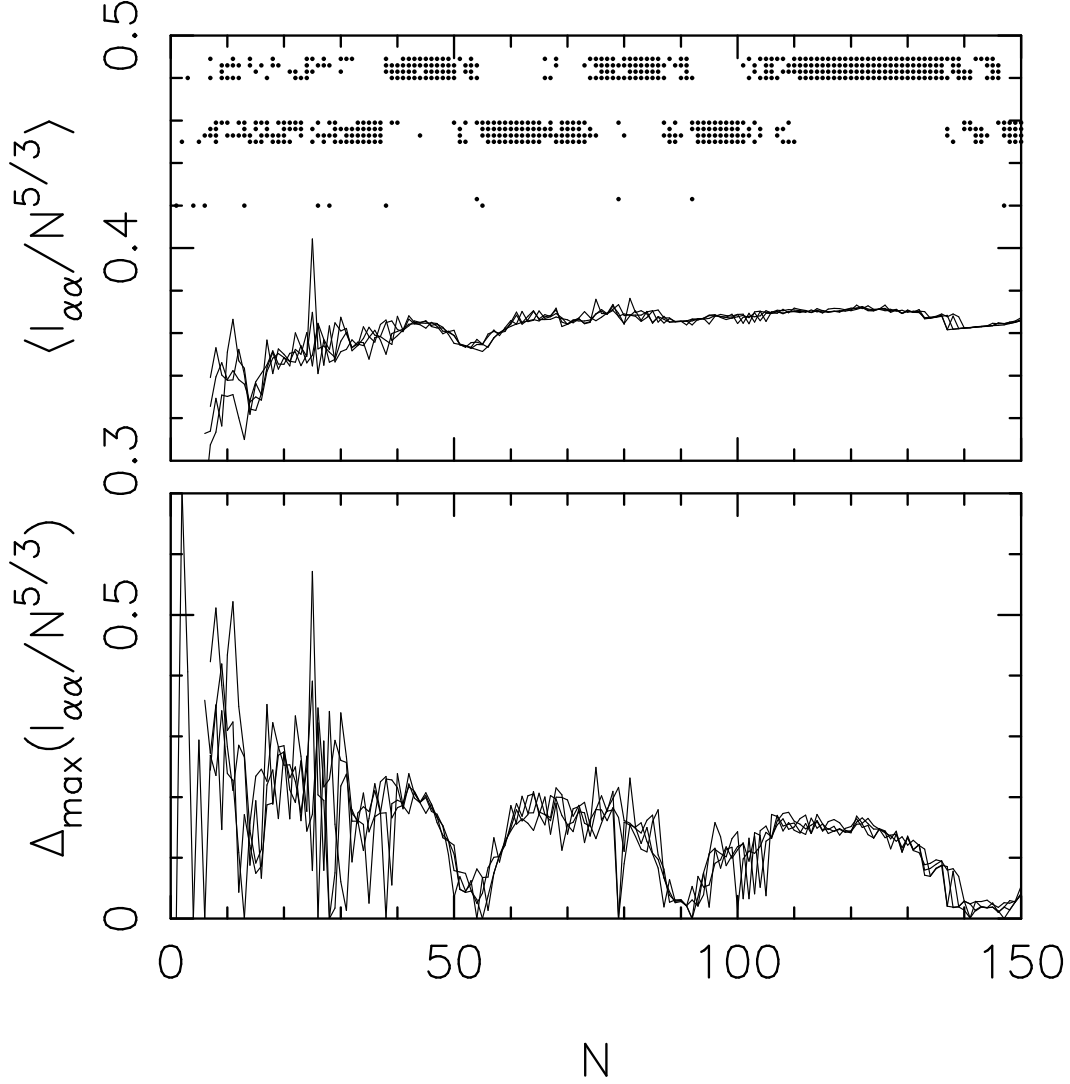


FIG. 5: Different properties related to the eigenvalues  $I_{\alpha\alpha}$ . In the upper panel we show the average value together with points indicating whether clusters with overall spherical shape (lowest set of rows), overall cigar shape (middle set of rows), or overall lens shape (upper set of rows) are found for a certain size. Moreover, in each set of rows, the lowest row corresponds to the energetically lowest isomer, the second one to the energetically second-lowest isomer, etc. In the lower panel we show the maximum difference of the eigenvalues for the four different isomers.

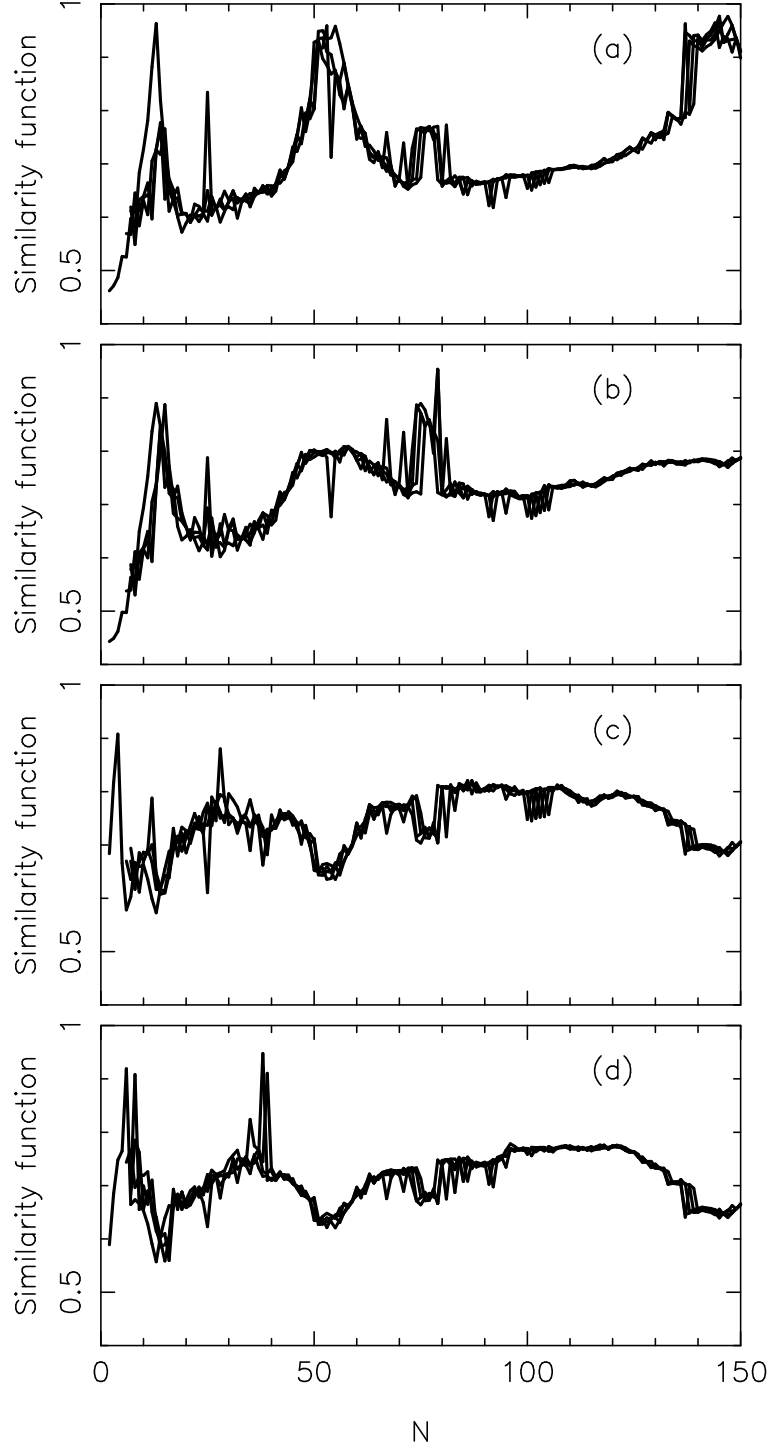


FIG. 6: Each panel shows the similarity function for all four isomers when comparing with (a) an icosahedral cluster, and (b–d) a spherical fragment of the *fcc* crystal when the center of the fragment is placed at (b) the position of an atom, (c) the middle of a nearest-neighbor bond, and (d) the center of the cube, respectively.



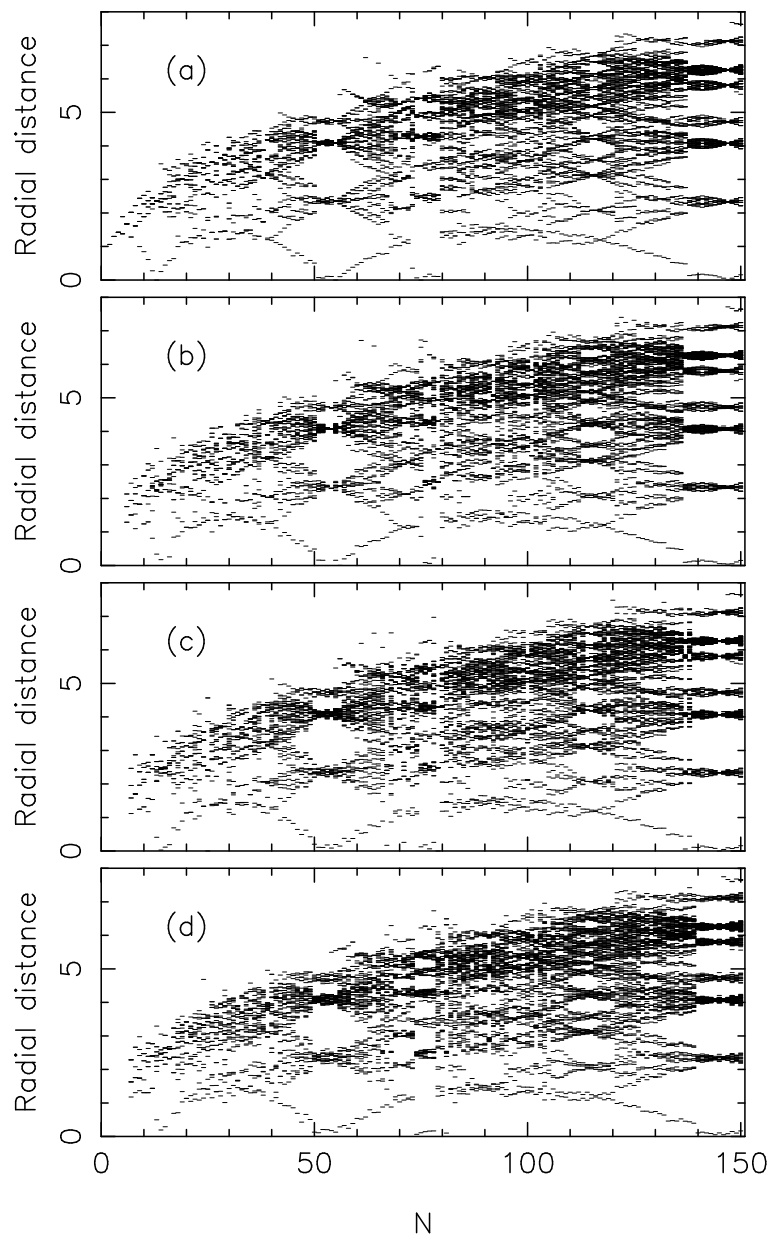


FIG. 7: Each panel shows the radial distances (in Å) as a function of cluster size, i.e., each small line represents (at least) one atom with that radial distance. The energy of the isomers increases from the top to the bottom.

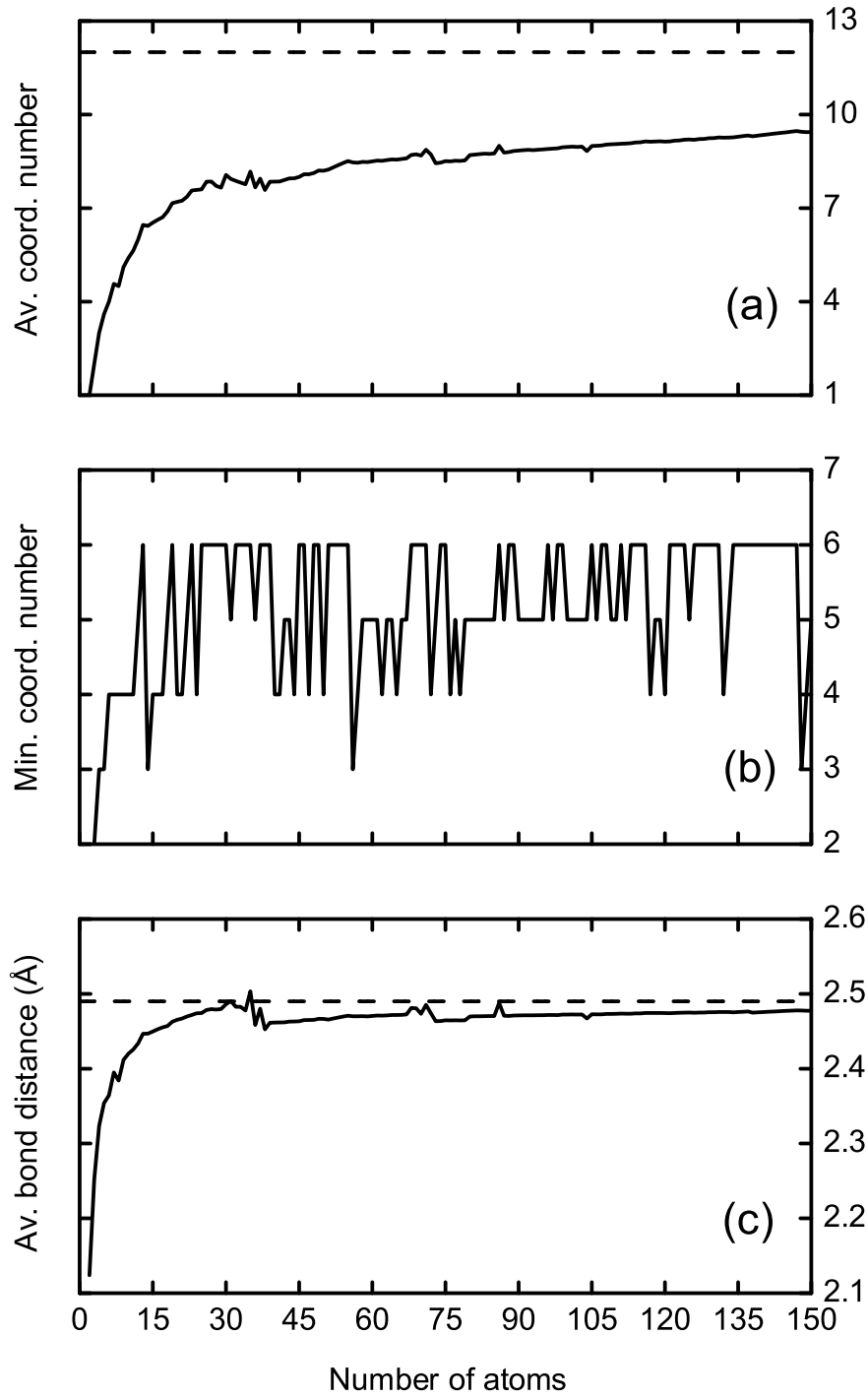


FIG. 8: (a) the average coordination number, (b) the minimum coordination number, and (c) the average bond distances as functions of cluster size. The dashed lines in (a) and (c) show the corresponding bulk values for nickel.

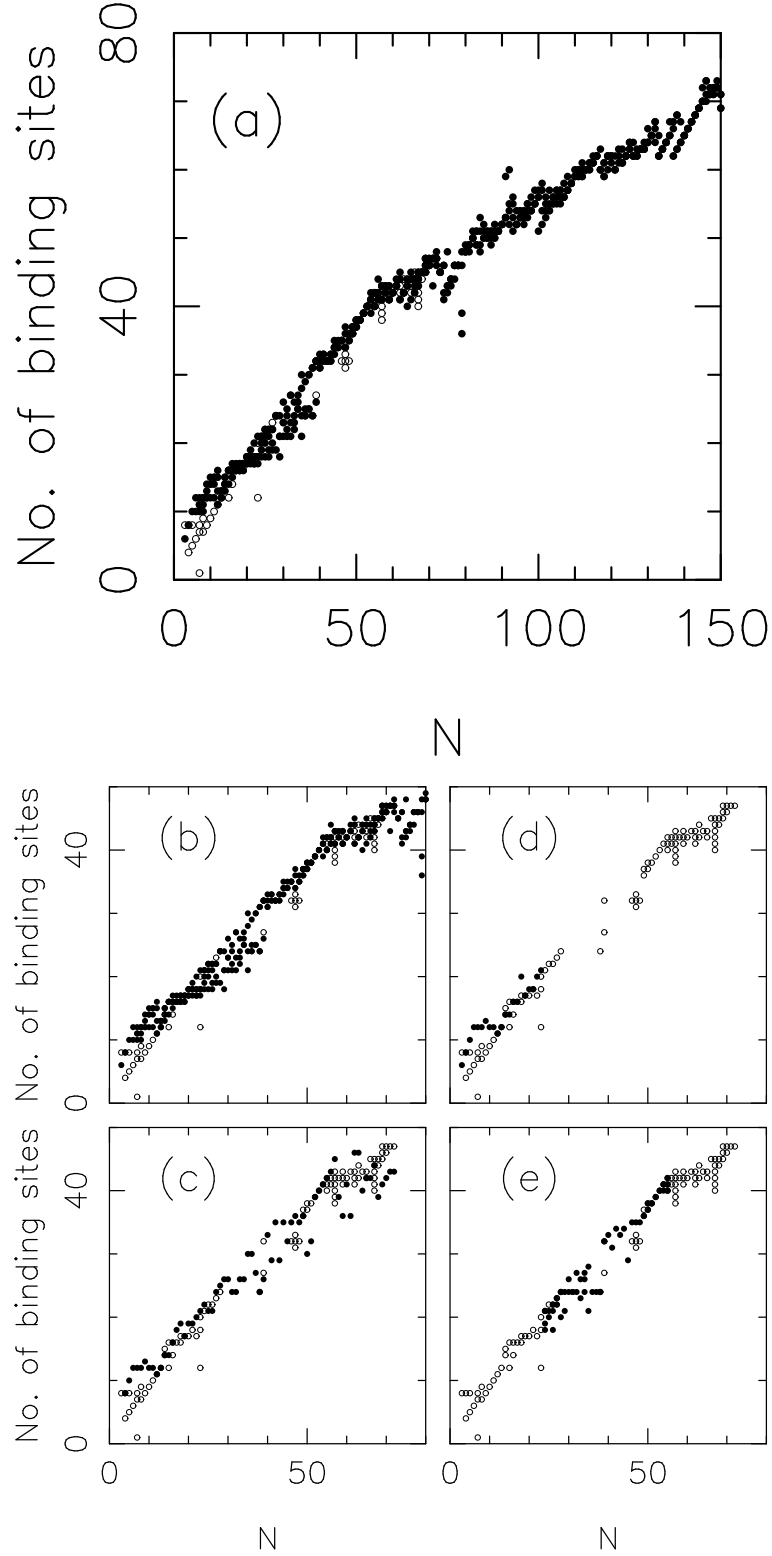


FIG. 9: The (open circles) experimentally determined number of  $N_2$  binding sites for  $Ni_N$  clusters from Refs. [33,34,35] as function of  $N$  in comparison with theoretical calculated numbers (closed circles) from (a,b) the present work, (c) from [23], (d) from [25], and (e) from [17].

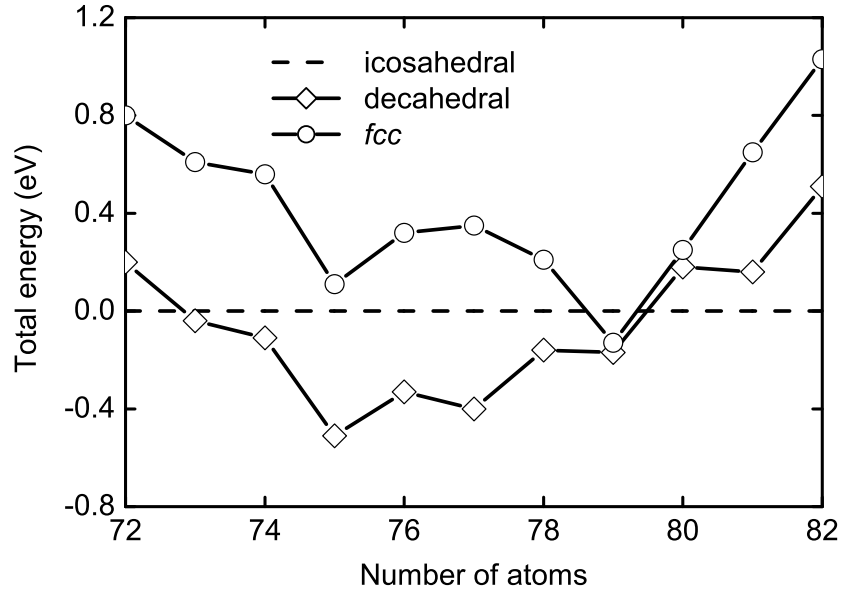


FIG. 10: The relative stability of the icosahedral, decahedral and *fcc* structures as function of cluster size for  $72 \leq N \leq 82$ .

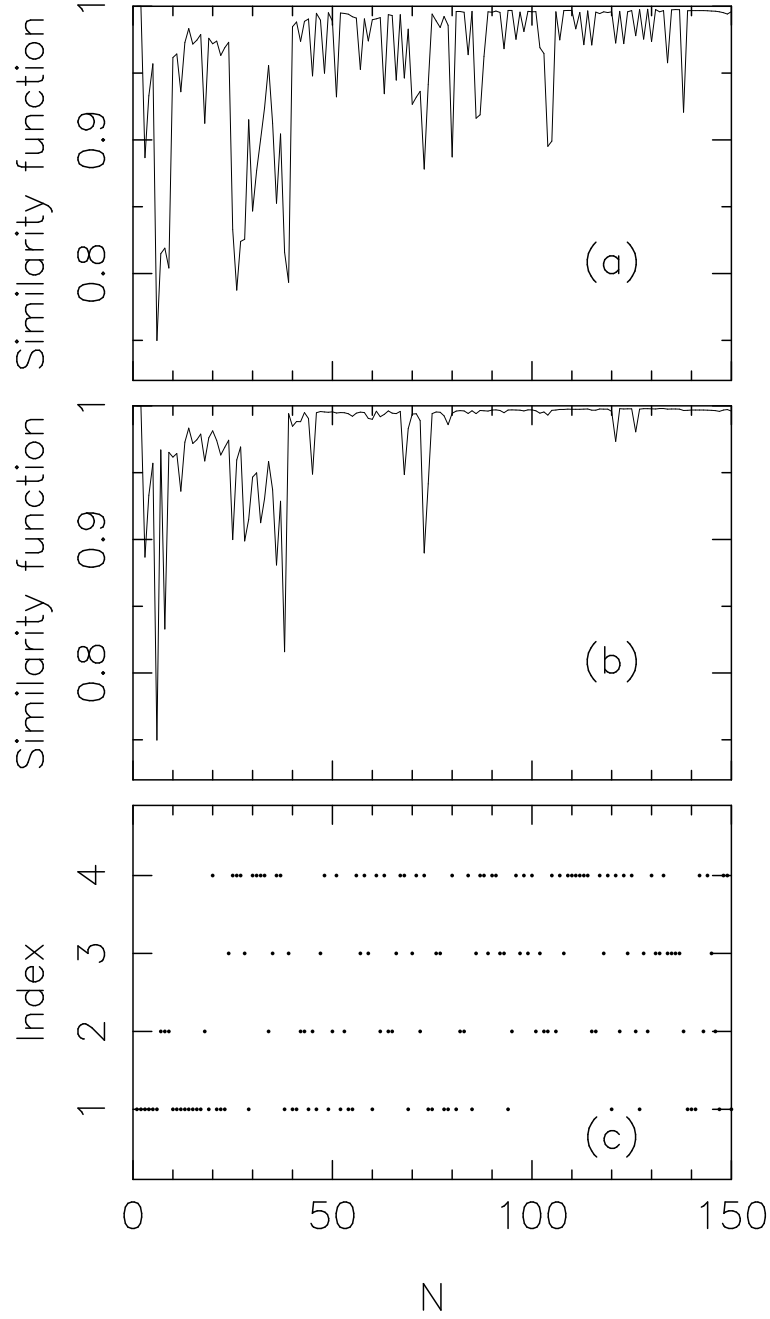


FIG. 11: (a) and (b) show the similarity functions that describe whether the cluster with  $N$  atoms is similar to that of  $N - 1$  atoms plus an extra atom, when (a) only considering the lowest-energy isomer for the  $(N - 1)$ -atom cluster and (b) considering all four isomers for that cluster. (c) shows which isomer in the latter case is most similar to the one of  $N$  atoms.